Lab-on-a-chip Technologies Enabled by Surface Acoustic Waves

XIAOYUN DING[a], PENG LI[a], SZ-CHIN STEVEN LIN[a], ZACKARY S. STRATTON[a], NITESH NAMA[a], FENG GUO[a], DANIEL SLOTCAVAGE[a], XIAOLE MAO[b], JINJIE SHI[a], FRANCESCO COSTANZO[a], THOMAS FRANKE[c], ACHIM WIXFORTH[d], AND TONY JUN HUANG*[a,b]

[a]Department of Engineering Science and Mechanics, The Pennsylvania State University, University Park, PA 16802, USA; [b]Department of Bioengineering, The Pennsylvania State University, University Park, PA 16802, USA; [c]School of Engineering, University of Glasgow, Glasgow G12 8LT, UK; [d]University of Augsburg, Augsburg, Germany
*E-mail: junhuang@psu.edu

15.1 Introduction

During the past two decades, microfluidics has emerged as an important platform in chemistry, biology, and medicine.[1–9] The introduction of "lab-on-a-chip" (*i.e.*, small-sized analytical devices) has spurred steadily increasing interest and research efforts in the microfluidics discipline (upon which lab-on-a-chip devices are based). The promise of such lab-on-a-chip devices is grounded in the advantages of microfluidics relative to traditional laboratory techniques used in chemistry and biomedicine: system miniaturization, automation, low cost, reduced reagent and sample consumption, rapid turnaround time, and precise microenvironment control. With an aim

to improve the functionality, versatility, and performance of lab-on-a-chip devices, researchers have continued to integrate new physics into the microfluidic platform. For example, the incorporation of electrowetting in microfluidics has enabled effective on-chip manipulation of droplets, *i.e.*, digital microfluidics.[10,11] Incorporation of magnetics in microfluidics has led to the demonstration of highly efficient cell manipulation and separation[12–14] and incorporating optics in microfluidics has spurred the development of fluid-based optical components such as optofluidic lasers, lenses, and modulators with unprecedented tunability.[15–19]

In recent years, surface acoustic wave (SAW) technologies have begun to receive significant attention in the microfluidics community. SAWs are acoustic waves that propagate along the surface of an elastic material. To date, SAW technologies have been used extensively in the telecommunication industry (*e.g.*, cell phones) for signal processing and filtering.[20] Other established applications of SAW technologies include touch-sensitive screens and biological/chemical sensing.[21–25] Recent research demonstrates that SAWs provide an effective means to control fluids and particles in lab-on-a-chip devices.[26] These SAW-based microfluidic devices offer the following useful and inimitable combination of features:

(a) Simple, compact, inexpensive devices and accessories: SAW devices have been used extensively in various compact commercial electronic systems, such as cell phones (each cell phone manufactured today contains multiple SAW devices which, along with their accessories, occupy only a small portion of the phone volume). This widespread commercial deployment demonstrates that SAW devices—and the accessories needed to drive them (such as driving circuits and power supplies)—are compact, inexpensive, and highly reliable.[20] SAW-based microfluidic devices would be simple and inexpensive to fabricate and integrate with other on-chip components in mass production.

(b) High biocompatibility: the acoustic power intensity and frequency used in many SAW-based microfluidic devices are both in a range similar to those used in ultrasonic imaging, which has been used extensively for health monitoring during various stages of pregnancy and proven to be extremely safe.[27] Therefore, we expect that with proper design, SAW-based microfluidic devices will also be safe and biocompatible with cells, molecules, and other biological samples. This expectation has been partially confirmed by cell viability and proliferation tests using existing acoustofluidic devices.[28–30]

(c) Fast fluidic actuation and large forces: current microfluidic technologies have difficulty generating fast fluidic actuation or large forces on particles. These drawbacks have limited their applications in medical diagnostics and biochemical studies. As indicated in a review article on microfluidics,[5] "small feature sizes typically prevent flow velocities from being high enough to yield high (Reynolds) numbers. High-frequency acoustic waves, however, can circumvent such difficulties." SAW-based devices can be used to selectively introduce chaotic

advection[31] to a microfluidic system (in which laminar flow generally dominates), thereby enabling fast, effective manipulation of fluids and particles. Thus far, SAW-based microfluidic devices have proven to be able to pump fluids at $1-10$ cm s^{-1} (ref. 31) and manipulate mm-scale objects (*e.g.*, *C. elegans*).[29] Neither of these two features can be readily achieved by other microfluidic techniques.

(d) Versatility: SAW technologies enable biological/chemical detection, fluidic control (*e.g.*, fluid mixing, translation, jetting, and atomization), and particle manipulation (*e.g.*, focusing, patterning, separation, sorting, concentration, and re-orientation). SAW technologies are capable of manipulating most microparticles, regardless of their shape, electrical, magnetic, or optical properties; they are capable of manipulating objects with a variety of length scales, from nm to mm; and they are capable of manipulating a single particle or groups of particles (*e.g.*, tens of thousands of particles).

(e) Contact-free manipulation: SAWs manipulate particles and cells by means of the primary acoustic radiation force applied by the surrounding fluid; and SAWs manipulate fluid by means of acoustic waves leaked into the fluid. This represents contact-free manipulation, eliminating the potential for sample contamination.

(f) Convenient on-chip integration with SAW-based sensors: SAW microfluidic devices can perform not only precise manipulation and control of both fluids and particles, but can also perform sensitive detection and sensing. SAW-based microsensors have matured over the years and can be integrated with other SAW-based microfluidic components.[21–23] These characteristics make it feasible to realize SAW-based, fully integrated, true lab-on-a-chip systems that can be launched into practical settings, rather than the chip-in-a-lab systems that we often encounter in the microfluidics community.

When compared with bulk acoustic wave (BAW) microfluidics,[33] another subset of acoustofluidics (*i.e.*, the fusion of acoustics and microfluidics), SAW microfluidics has its advantages and limitations. While BAW microfluidics is more mature, better understood, and has demonstrated higher throughput, SAW microfluidics has the following advantages:

(a) It allows one to better control excitation frequencies in a wider range and utilize higher excitation frequencies whenever needed. As a result, SAW microfluidics is more versatile and flexible and can achieve more precise and controllable manipulation of fluids and particles.

(b) It does not require that fluid channels be made of materials with high acoustic reflection, making it possible to employ microfluidic devices made of polymers, which generally have low acoustic reflection.

(c) Because SAWs confine most of their energy to the surface of a microfluidic device substrate (whereas BAWs expend energy travelling through the bulk of the device substrate), they require less power than BAWs to achieve the same acoustic effects.

(d) SAW devices can be conveniently fabricated on the same chip as many other microfluidic components through standard micro/nano fabrication processes in a mass-producible fashion. In this regard, SAW microfluidics appear to be more amenable to system integration and mass production than BAW microfluidics.

These recognized features and advantages of SAW microfluidics (relative to BAW microfluidics and other microfluidic approaches) have rendered it an attractive platform for many lab-on-a-chip applications. Although some aspects of SAW microfluidics have been reviewed elsewhere[34–39] (such as travelling SAW based droplet microfluidics, SAW based particle manipulation, and SAW based biosensing in microfluidics), we provide in this book chapter a comprehensive review of SAW microfluidics. We propose the decomposition of SAW microfluidics into two types: travelling SAW (TSAW) and standing SAW (SSAW). For both SAW types, we first introduce the theory before summarizing microfluidic applications to date. Finally, we look forward to identify areas with space for research innovations.

15.2 Travelling Surface Acoustic Wave (TSAW) Microfluidics

15.2.1 Theory Involved with TSAW

The best known form of SAW, Rayleigh SAW, is composed of a longitudinal and a vertically polarized shear component.[38] Rayleigh SAW strongly couples with media in contact with the wave propagation surface, enabling the sensing of mass perturbation and elastic properties of a medium introduced on the wave's propagation path. Other SAW modes exist in elastic materials of different compositions. For example, Love SAW is a guided shear-horizontal wave that propagates in a thin layer on top of a substrate. However, as most SAW-based lab-on-a-chip technologies utilize Rayleigh SAWs, we use "SAW" to specifically indicate Rayleigh SAW in this review.

SAWs are generally produced by applying an appropriate electric field to a piezoelectric material. The piezoelectric material, in turn, generates propagating mechanical stress. A typical SAW device uses at least one set of metallic interdigital transducers (IDTs) fabricated on the surface of a piezoelectric substrate. The IDT then introduces the electric field, generating a SAW displacement amplitude on the order of 10 Å. An IDT consists of a set of connected metallic fingers interspaced with an opposite set of connected metallic fingers; an alternating current electrical signal in the radio frequency (RF) range is applied across the two sets of connected fingers (Figure 15.1). The structure of the IDT determines the bandwidth and directivity of the generated SAW. By changing the number, spacing, and aperture (overlapping length) of the metallic fingers, one can change the characteristics of the resulting SAW. For example, a focused IDT consists of pairs of annular electrodes that can focus SAW energy to a spatially small

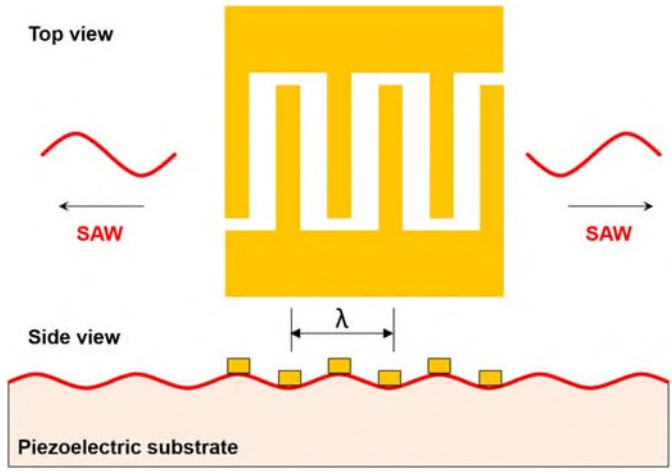

Figure 15.1 A metallic IDT deposited on the piezoelectric substrate generates SAWs that propagate along the substrate surface in both directions.

focal point.[40] A chirped IDT has a gradient of the electrode finger width directed along the SAW propagation direction, allowing it to generate SAWs over a wide frequency range.[29] A slanted finger IDT has a gradient of electrode finger width directed perpendicular to the SAW propagation direction, allowing it to generate narrow SAW beams of varying frequency along its finger length.[41] Each IDT variant has its own set of advantages and disadvantages and the choice of IDT type for use in a SAW-based microfluidic device depends on the device requirements. Additional IDT design types will be discussed in the later portion of this review article.

Generation of SAWs on a piezoelectric material can be mathematically modeled, but is complicated by (1) the anisotropy exhibited in most piezoelectric materials and (2) the intrinsic electromechanical coupling in piezoelectric media. The anisotropy of a piezoelectric material dictates whether the piezoelectric material generates shear-horizontal SAW,[42] leaky SAW,[43] or psuedo-SAW.[44] As such, consideration must be given to anisotropy to ensure the generation of the desired type of wave. The full mathematical modeling of SAW propagation requires the analysis of the link between electrical signal and deformation in piezoelectric media, referred to as electromechanical coupling.[45–72] For more details on theory, see Chapter 14.

15.2.2 Microfluidic Technologies Enabled by TSAWs

In this section, we review the application of TSAWs in both open and confined microfluidic geometries to accomplish (1) fluid mixing, (2) fluid translation, (3) jetting and atomization, (4) particle/cell concentration, (5) droplet and cell sorting, and (6) re-orientation of nano-objects. These examples demonstrate the growth of TSAW into a key component for many emerging on-chip applications.

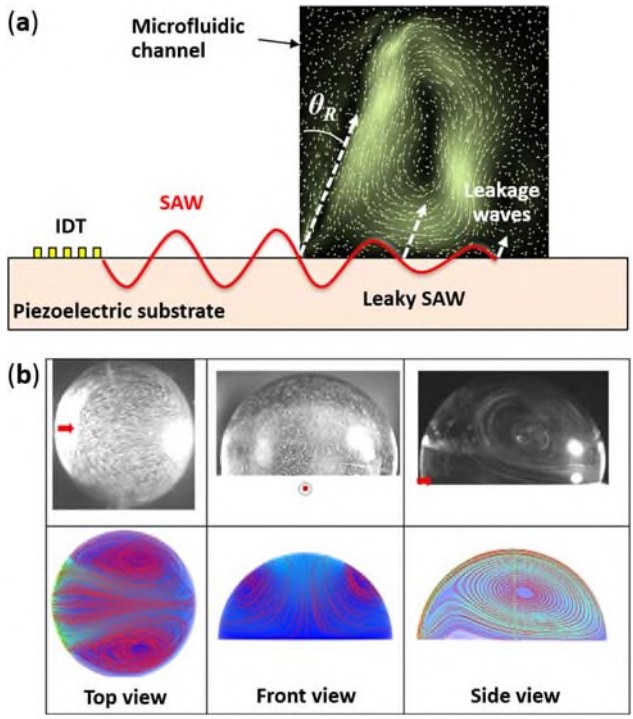

Figure 15.2 SAW-induced acoustic streaming. (a) Rayleigh SAW is excited by means of an IDT. Underneath a liquid, the SAW turns into a leaky SAW, radiating pressure waves at the Rayleigh angle θ_R into the fluid. The streaming map is from Koster. Reprinted with permission from ref. 46. (b) Comparison of experimental results and numerical modeling for a hemispherical droplet positioned at the center of the SAW propagation direction. Reprinted with permission from ref. 52.

15.2.2.1 Fluid Mixing

Many lab-on-a-chip applications require the mixing of two or more fluids. However, the laminar flows that predominate at the micro-scale result in mixing that occurs *via* diffusion. Such diffusion-based mixing is too slow for most lab-on-a-chip applications, so researchers have looked to SAW-induced streaming for its ability to mix fluids quickly by generating chaotic advection (Figure 15.2).

A few groups have demonstrated methods using TSAWs to mix fluids in an unconstrained droplet. Shilton *et al.*[56] generated a TSAW using a single-phase unidirectional transducer (SPUDT) to induce liquid recirculation inside a droplet. Their results, shown in Figure 15.3(a), demonstrate the fast mixing of dyed water and dyed glycerin solution. Frommelt *et al.*[73] demonstrated a more refined TSAW-based droplet mixing, using a pair of tapered IDTs (TIDTs) to generate a narrow SAW beam with a tunable launching point.

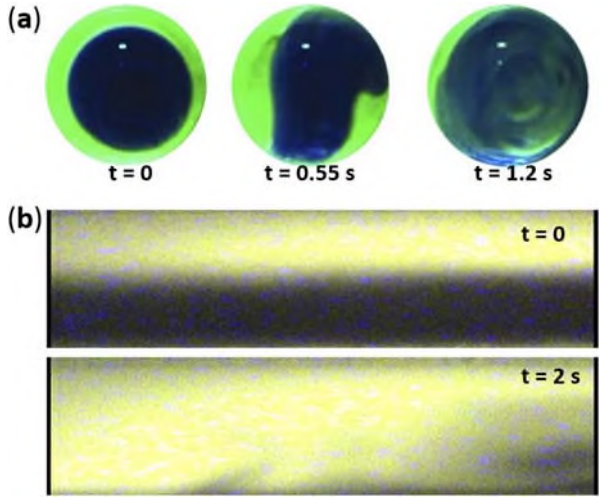

Figure 15.3 Fluid mixing by SAW-induced acoustic streaming. (a) Rapid mixing of glycerin (light) and water (dark) in a droplet. (b) Mixing of fluorescence dyes (light) with water (dark) in a rectangular microfluidic channel. Reprinted with permission from refs. 56 and 54.

By individually modulating the input signals of the two TIDTs, they demonstrated the ability to temporally modulate the flow patterns generated by each IDT to achieve efficient mixing. They also demonstrated that they could control mixing speed (within the droplet) by adjusting SAW amplitude and frequency.

Tseng *et al.*[54] also used IDTs to demonstrate TSAW-based mixing. Instead of mixing fluids in an unconstrained droplet, they mixed fluids inside a microchannel (Figure 15.3(b)). They performed a comprehensive experimental study on the effects of various operational parameters, showing that mixing performance could be significantly improved by applying higher voltage signals to the IDTs. Luong *et al.*[74] used a curved IDT design to focus the generated acoustic energy, resulting in considerably improved mixing performance relative to the parallel IDT design employed by previous groups.

Recently, Rezk *et al.*[75] incorporated SAW-induced mixing in a paper-based microfluidic device. They utilized a hue-based colorimetric technique to compare the mixing efficiency of their device with that of capillary-based mixing: the SAW-based mixing showed greatly enhanced consistency and speed.

By adjusting IDT design and input signal parameters, researchers have proven that TSAWs can effectively and precisely mix fluids in both open and confined fluid geometries. This versatility makes TSAW-based mixing techniques extremely attractive in microfluidics.

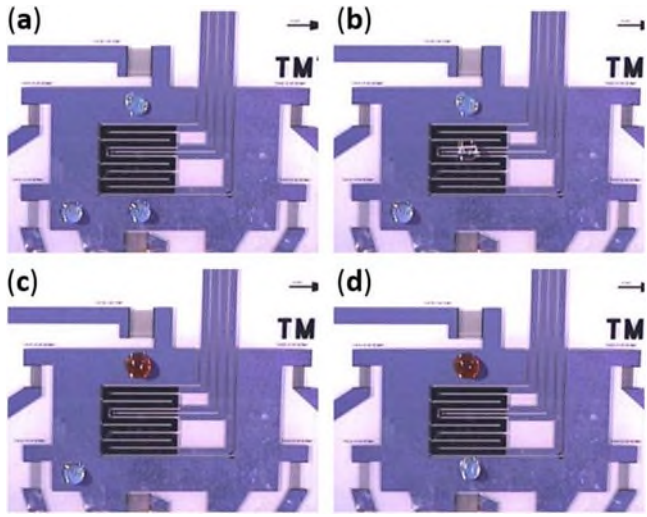

Figure 15.4 TSAW-driven programmable bioprocessors. (a–d) Three droplets are moved individually and with precise control. Reprinted with permission from ref. 78.

15.2.2.2 Fluid Translation

15.2.2.2.1 Fluid Translation in Open Space

When a liquid droplet is placed within the propagation path of TSAWs on a piezoelectric substrate, leaky SAW will be diffracted into the droplet at the Rayleigh angle. If the SAW has low amplitude, it will induce acoustic streaming within the droplet. If the SAW has sufficiently intermediate amplitude, the leaky acoustic energy generates an acoustic force on the droplet along the SAW propagation path, causing the droplet to deform into an axisymmetrical conical shape and translate across the substrate.[49,76,77] Liquid droplet speeds of 1–10 cm s^{-1} can be achieved using this TSAW-based actuation; this is more than an order of magnitude faster than other current micro-pumping actuation schemes.[32]

Moreover, as electrical actuation of IDTs can be programmed, droplet movements can be automated. Through the automated control of multiple droplets, merging, mixing, splitting, and chemical or biochemical reactions can be performed in so-called "programmable bioprocessors". A simple example of a programmable bioprocessor is shown in Figure 15.4, in which three droplets with different fluid content are moved independently in any desired direction and can be made to join together.[78]

Many chemical and biological applications have been demonstrated with TSAW-driven droplets. Guttenberg *et al.* precisely actuated oil-covered aqueous droplets between sinkers and heaters to perform a highly sensitive, fast, and specific DNA amplification reaction with droplet volumes as low as 200 nL.[79] Similarly, Tan *et al.* rapidly and effectively collected and removed

micro-particles using this TSAW-driven droplet translation technique.[80] Finally, Li *et al.* used a similar mechanism to transport cells into tissue scaffolds to enhance cell seeding for tissue engineering studies.[81]

Rezk *et al.* subjected a droplet of silicone oil to TSAW excitation, observed behavior substantially different from that of water droplets, and developed a theory for the behavior (Figure 15.5(a)).[82] Silicone oil has a much smaller contact angle with a $LiNbO_3$ piezoelectric substrate than does water. When a silicone oil droplet on such a substrate was exposed to TSAW, this small contact angle led to the majority of the droplet being propelled in the SAW propagation direction (Figure 15.5(b)), while a thin film spread in the opposite direction (Figure 15.5(c)). As the thin film advanced, it formed finger-shaped patterns (Figure 15.5(d)); eventually, soliton-like wave pulses appeared above the fingers and propagated along the TSAW direction

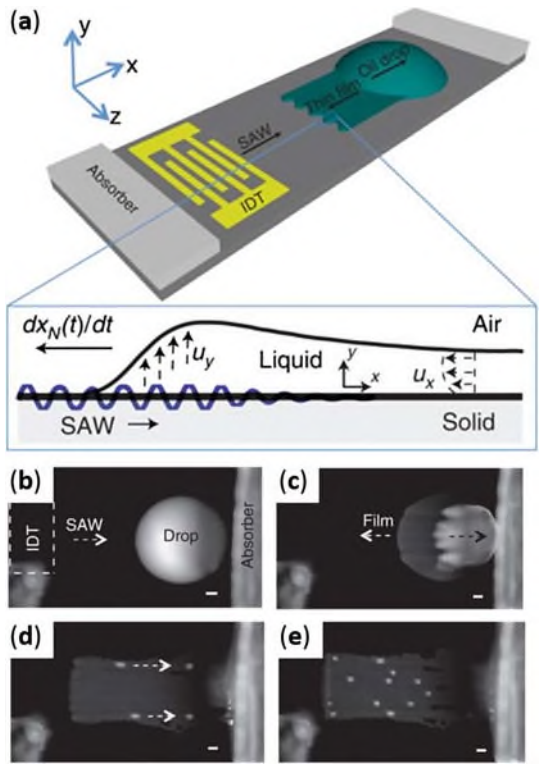

Figure 15.5 (a) Schematic of experimental setup depicting the emergence of a thin film from a standing oil drop due to TSAW exposure. (b) Initial state of the oil droplet. (c) After excitation with TSAW, the bulk of the oil droplet is displaced along the SAW propagation direction while a thin oil film advances in the opposite direction. (d) Finger patterns form in the thin film. (e) Soliton-like wave pulses subsequently appear above the fingers and translate in the SAW propagation direction. Reprinted with permission from ref. 82.

(Figure 15.5(e)). The authors suggest that this TSAW-induced thin film spreading may have applications in film coating and microfluidic actuation.

Historically, most SAW microdevices have been fabricated on bulk $LiNbO_3$ or quartz substrates; these bulk piezoelectric substrates may require some extra processing in order to integrate control electronics (*e.g.*, for the IDTs). To facilitate further advancements in SAW microfluidics, Du *et al.* presented a thin film piezoelectric material for translation of liquid droplets with volumes up to 10 μl.[53] They first deposited a ZnO thin film on a plain silicon substrate. This hydrophilic ZnO thin film layer prevents effective droplet translation. To circumvent this, they treated the ZnO thin film with a self-assembled monolayer of octadecyltrichlorosilane (OTS), which made the substrate surface hydrophobic while producing no measurable acoustic damping. The new substrate is cheaper than bulk piezoelectric substrates, and the silicon base can easily be integrated with control electronics for the IDTs, enabling the potential for a fully automated microsystem.

15.2.2.2.2 Microfluidic Pumping in Enclosed Channels

In addition to translating liquid droplets in open space, TSAWs can be employed to pump fluid through enclosed channels.[83–89] Cecchini *et al.*[86] bonded a straight PDMS microchannel between two IDTs on a $LiNbO_3$

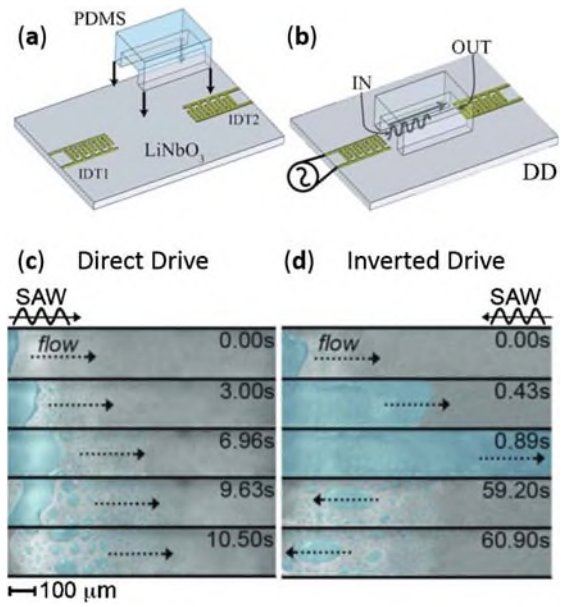

Figure 15.6 (a) Schematic of the assembly of the microfluidic device and (b) activation of IDT1, called direct drive (DD) mode; activation of ID2, called inverted drive (ID) mode, results in TSAW propagation opposite that shown in this image. (c) Photographs of the (ineffective) water filling process under DD mode at different times. (d) Photographs of the water filling process under the ID mode at different times. Reprinted with permission from ref. 86.

substrate (Figure 15.6(a)). After placing a water droplet between one IDT and the channel inlet (this droplet was termed the water "reservoir"), two different operation modes were tested: direct drive mode and inverted drive mode. In direct drive mode, SAWs were excited by the IDT near the channel inlet and propagated from inlet to outlet (Figure 15.6(b)), whereas inverted drive mode had SAWs excited by the IDT near the channel outlet and propagated from outlet to inlet. In direct drive mode, SAW excitation caused significant atomization in the water reservoir, resulting in rapid evaporation of the water and preventing the channel from being filled (Figure 15.6(c)). In inverted drive mode, the water reservoir quickly translated into the microchannel, filling it at a flow speed as high as 1.24 mm s^{-1}. The authors propose that this flow rate, occurring opposite the TSAW propagation direction, is attributable to TSAW-induced atomization at the leading edge of the water. These droplets continuously form, coalesce, and rejoin the water–air meniscus, thereby dragging the water through the channel and resulting in net motion opposite the direction of TSAW propagation (the water reservoir is not exposed to significant atomization under the inverted drive configuration because the TSAW power is sufficiently diminished by the time it reaches the reservoir location at the channel inlet).

Based on this TSAW inverted drive mechanism, Girardo *et al.*[87] developed a fully controlled low-voltage micro pump in a two-dimensional microchannel array. By combining a 5 × 5 orthogonal array of PDMS microchannels on a $LiNbO_3$ substrate with 20 IDTs, the researchers could selectively generate either a single TSAW or multiple TSAWs. Thus, droplets at channel inlets could be directed through the microchannel grid to the desired outlets. This device achieved several SAW-driven fluid operations including extraction, deviation, splitting, and simultaneous multichannel filling.

TSAW-driven pumping has also been demonstrated in a closed microfluidic channel (with no liquid–air interface) by Fallah *et al.*[88] This device featured a microfluidic channel in a square-shaped loop, with an IDT to generate SAWs travelling along one of the four sides. When a TSAW reaches the fluid–substrate interface, the acoustic energy leakage profile decays exponentially with continued wave travel along the fluid channel. With a sufficiently long channel, the location of initial TSAW contact with the fluid essentially acts like a point pressure source, driving the fluid through the channel loop according to conservation of mass. With this setup, fluid flow could be continuously actuated with a very fast response. Fluid pumping in such a closed-loop chamber can be used to mimic the action of small blood vessels, making it useful for clinical applications and biomedical studies.[83,84,89]

15.2.2.2.3 Microfluidic Rotational Motor

Shilton *et al.* utilized SAW-induced acoustic streaming to drive a rotary micromotor in a microfluidic chip (Figure 15.7(a)).[90,91] A pair of IDTs were patterned on a $LiNbO_3$ substrate, and a layer of hydrophobic Teflon film was coated in the space between the two IDTs in order to hold a fluid droplet in

place. Silicone gel was placed on the SAW's path to absorb half of the energy from each IDT, creating a centrosymmetric TSAW exposure in the droplet, which resulted in centrosymmetric acoustic streaming inside the droplet. When a Mylar disc with a 5 mm diameter and 100 μm thick was placed on top of the droplet, the droplet's rotational inertia actuated rotational motion in the disc (shown in Figure 15.7(b)). The disk's angular velocity under a range of SAW amplitudes was investigated. In the case in which a 50 μl water drop was used as the fluid-coupling layer, a maximum disk rotation speed of 2250 rpm was achieved with a maximum torque of around 69 nNm. The authors found that increasing SAW amplitude to surpass ~3 nm would reduce angular speed due to the unstable disc rotation caused by asymmetric flow in the drop.

By replacing the original Mylar micromotor with a patterned disk, Glass *et al.* successfully used this setup as a miniaturized lab-on-a-disc.[92] These discs were patterned with microfluidic channels, enabling SAW-induced microcentrifugation. With this setup, the authors demonstrated functions such as capillary valving, mixing, and particle concentration and separation.

As described in the above examples, SAW-induced acoustic streaming enables a simple and miniaturized on-chip rotational motor without the need for moving mechanical parts. In future studies, researchers will likely examine fluid-coupling layers other than water in order to circumvent the potential for evaporation.

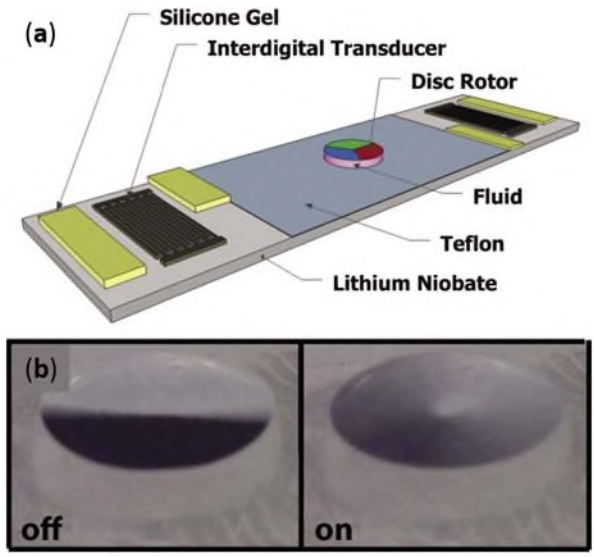

Figure 15.7 (a) Schematic of the SAW-induced rotary micromotor. Silicone gel was used to break the axisymmetry of the planar SAW and generate a centrosymmetric SAW, resulting in centrosymmetric acoustic streaming inside the drop. (b) The static and spinning states of the Mylar disc placed on top of the drop. Reprinted with permission from ref. 90.

15.2.2.3 Jetting and Atomization

A fluid jet is commonly defined as a coherent stream of fluid projected into a surrounding medium. For a fluid to undergo jetting phenomena, it must possess sufficient inertia to overcome the restoring capillary forces acting on the interface of the fluid and surrounding media.[31,93] Jetting at micro-scales finds numerous applications in hand-held ink jet printers, ink jet highlighters, and ink jet brushes.[94,95] Such micro-scale jetting can be accomplished by exposing small fluid volumes to TSAW (with the SAW power higher than that used for droplet translation), Figure 15.8. Recent research has demonstrated that SAW-based fluid jet production offers benefits over existing jetting techniques as it concentrates mechanical energy into a small drop, generating jets without the narrow confinement typically necessary to accelerate fluid.

Recently, Tan *et al.*[96] studied the nature of jet formation using TSAW devices, as shown in Figure 15.8. They characterized jetting length as a function of the driving force and the jet Weber number. They also predicted the jet's velocity as a function of acoustic Reynolds number using the jet momentum equation of Eggers,[93] and verified their results with the experimental data. These rigorous characterization efforts have helped to facilitate future TSAW-based jetting technologies.

Atomization is the making of an aerosol of small solid particles or liquid droplets. It has long been applied in numerous areas, such as internal combustion engines, medicine, agriculture, and cosmetics.[97] Kurosawa *et al.* first proposed and constructed a novel ultrasonic atomizer using a TSAW device.[98] Since then, SAW-based atomization has been used for numerous applications such as protein extraction and characterization for paper-based diagnostics,[99] portable pulmonary delivery of asthmatic steroids,[100] and mass spectrometry interfacing with microfluidics.[101,102] Qi *et al.*[103] proposed a miniature inhalation device based on SAW atomization, and Ho *et al.*[104] merged SAW atomization with a paper-based sample delivery system to detect the presence of caffeine in human whole blood.

TSAW atomization has also been utilized for producing micro and nano particles. Alvarez *et al.*[105] demonstrated the generation of protein aerosols and nanoparticles using SAW atomization, while Friend *et al.*[106] utilized a similar technique to synthesize polymeric nanoparticles. The small footprint of its

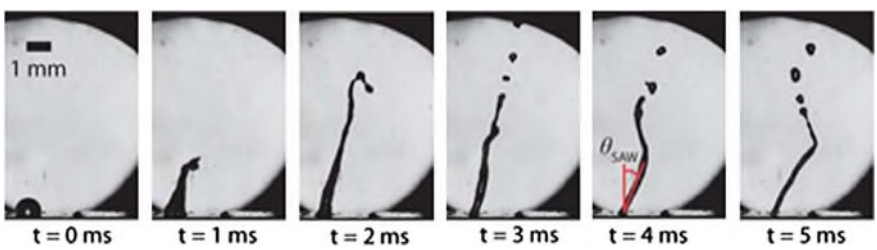

Figure 15.8 Jetting generation resulting from exposure to travelling SAW. Reprinted with permission from ref. 96.

generating mechanism, low power consumption, biocompatibility, and control over aerosol size make SAW an attractive method for atomization and a potential enabler for next-generation drug delivery devices.

TSAW-induced atomization is a result of capillary waves on the air–liquid interface.[107] The mathematical analysis of this phenomenon is challenging due to the presence of a free interface and a non-linear, two-dimensional wave interaction coupled with vastly varying time scales. Despite the associated difficulty, numerous efforts have been made to understand this phenomenon from a theoretical perspective. Köster[57] used a perturbation approach to investigate flow field inside a droplet, while Dong *et al.*[108] approached the problem by solving three-dimensional Navier–Stokes equations using a volume-of-fluid method to determine the free interface. Tan *et al.*[109] used a coordinate transformation approach to model the deformation of the interface, deriving the bulk deformation and unsteady capillary wave from the most basic principles, thus allowing their approach to correctly calculate acoustic wave reflections. Most recently, Collins *et al.*[110] investigated the hydrodynamics associated with SAW atomization, and developed a model for thin film spreading behavior under SAW excitation. Despite recent progress in describing the physics governing SAW-induced atomization, much remains to be understood.

15.2.2.4 Particle/Cell Concentration

Concentrating particle/cell suspensions is a basic but critical operation in many applications in chemistry and biomedicine. On the macro-scale, particles can be easily concentrated using centrifugation. On the micro-scale, however, concentrating cells or particles can be difficult. As volume decreases, surface forces acting on the particles/cells begin to dominate over body forces. Lack of significant body forces makes standard centrifugation impractical, so researchers have explored SAW-induced acoustic streaming to concentrate cells and particles for low-volume systems.[56,111–113]

To initiate rotational fluid motion, Shilton *et al.*[56] placed a droplet within a portion of a SAW propagation pathway in such a way that the droplet experienced TSAW exposure across a fraction of its width. This resulted in a circular pattern of SAW-induced acoustic streaming within the droplet (Figure 15.9(a)). When microparticles in aqueous suspension were subjected to this rotational pattern of SAW-induced streaming, they were concentrated and deposited in the center of the droplet. The researchers attributed the concentration effects to a shear gradient between regions of high shear at the droplet's periphery and regions of low shear at the droplet's center. Particles tended to move towards the region of low shear, where the linear velocities of the fluid approached zero.

Figure 15.9(b) shows sequential images of the SAW-induced streaming for a water sample containing 0.5 μm white fluorescent beads. The progression from distributed individual dots at $t = 0$ to the central bright spot at $t = 1$ s demonstrates how quickly the rotational SAW-induced streaming moves the

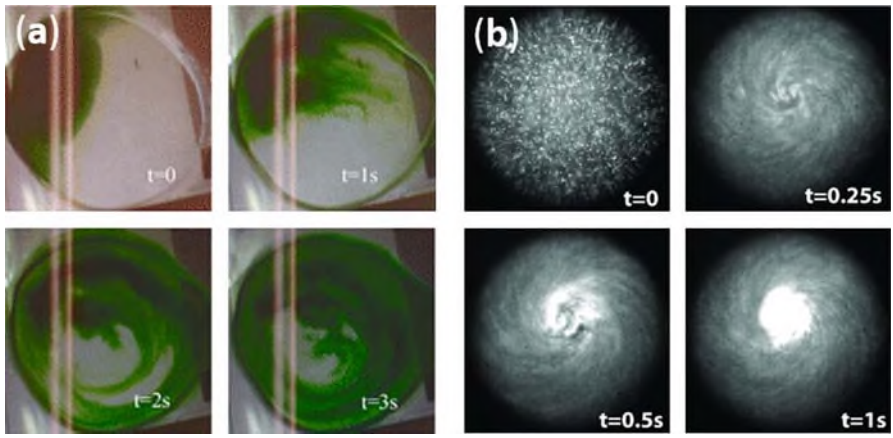

Figure 15.9 (a) Sequential images of rotational acoustic streaming in a drop resulting from asymmetric exposure to TSAWs, with flow streamlines visualized using dye. (b) Concentration of particles in a 0.5 μl droplet *via* such rotational acoustic streaming. Reprinted with permission from ref. 56.

fluid and concentrates the particles. In this way TSAWs allow for quick and efficient particle concentration at the micro-scale with a simple droplet-based device setup.

15.2.2.5 Droplet/Cell Sorting

The ability to precisely sort individual droplets of interest from other droplets is extremely important for various chemical and biological screenings. Similarly, cell sorting is an important task for many disciplines, ranging from basic cell biology to clinical diagnosis. Recently, several groups have shown that SAW-induced acoustic streaming can selectively sort droplets or cells.[114–116] More details on this subject are to be found in Chapter 16.

15.2.2.6 Reorientation of Nano-objects

15.2.2.6.1 Carbon Nanotube Alignment

Carbon nanotubes (CNTs) have been a focus of nanotechnology research for over two decades.[117] Their mechanical strength and unique electrical properties make CNTs attractive for a wide variety of applications ranging from sports equipment to electronics. However, aligning large quantities of CNTs for use in these applications often proves challenging. TSAWs present a practical solution, allowing for the simultaneous alignment of many CNTs.

Strobl *et al.* demonstrated the alignment of multi-walled carbon nanotubes (MWNTs) on a $LiNbO_3$ substrate using TSAWs.[118] Figure 15.10(a) shows a typical setup for the SAW-induced nanotube alignment device. After activating the SAWs, the device aligned carbon nanotubes 25−45° relative to the SAW field (shown in Figure 15.10(b)). To discern between the effects of fluid

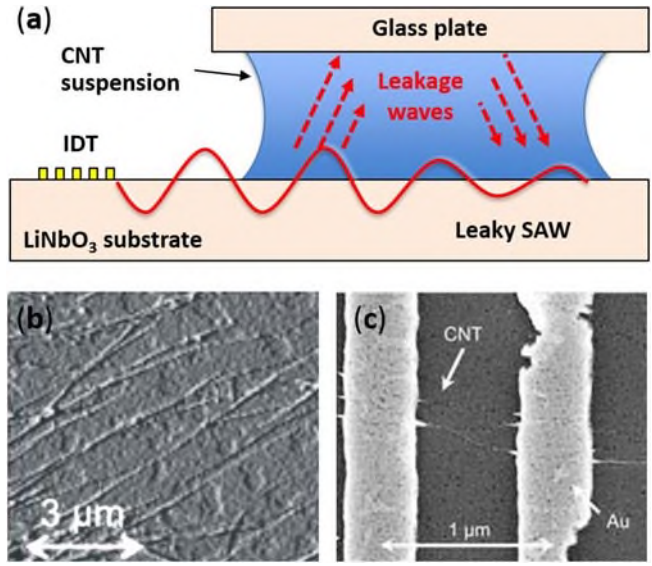

Figure 15.10 (a) Schematic of device setup for SAW-based carbon nanotube alignment. (b) AFM image of aligned multi-walled carbon nanotubes. Reprinted with permission from ref. 118. (c) SEM image of aligned single-walled carbon nanotubes between pre-patterned gold electrodes on $LiNbO_3$. Reprinted with permission from ref. 119.

movement and piezoelectric field in the alignment of these MWNTs, the authors covered the $LiNbO_3$ substrate with a 20 nm layer of NiCr. This thin metallic film then screened the piezoelectric field of the TSAWs. Experiments conducted on this metal-coated substrate device yielded no observable alignment of the MWNTs. To confirm this observed alignment is dependent on the piezoelectric field, the authors then used a $LiTaO_3$ substrate to propagate a shear-wave SAW (as opposed to the Rayleigh SAW propagated on a $LiNbO_3$ substrate). The mechanical component of a shear-wave SAW exists in the plane of the crystal, yielding minimal fluidic coupling relative to that of Rayleigh SAWs. When using $LiTaO_3$ substrate, the MWNTs aligned parallel to the SAW field, showing improved alignment relative to the $LiNbO_3$ device. Thus the authors concluded that the MWNT alignment is attributable to the piezoelectric field associated with SAW propagation, and the acoustic streaming generated by Rayleigh SAWs actually shifted the MWNTs from being directly aligned with the piezoelectric field.

Smorodin *et al.* improved upon the alignment performance of the SAW-only approach by first thiolating single-walled carbon nanotubes (SWNTs) and then placing them on a substrate with patterned gold electrodes (Figure 15.10(c)).[119] By applying SAWs across this setup, the authors found that a majority of SWNTs aligned at angles between 0 and 20° relative to the SAW field. They attributed this improvement to the rapid attachment of thiolated carbon nanotubes to the gold electrodes, reducing the impact of acoustic streaming on the nanotube alignment.

Though the previous studies demonstrated successful alignment of CNTs, their use of piezoelectric substrates limits their usefulness in microelectronics applications, as most microelectronic devices use non-piezoelectric silicon substrates. Seemann *et al.* used a "flip-chip" configuration to overcome this limitation, enabling the alignment of carbon nanotubes on a silicon substrate.[120] In the experiment, a silicon substrate was patterned with gold contacts and then brought into close proximity with a $LiNbO_3$ substrate. A CNT solution was deposited to fill the space between the two substrates. Application of TSAWs to the CNT solution (by means of the $LiNbO_3$ substrate) resulted in a combination of piezoelectric field and acoustic streaming effects that successfully aligned CNTs between the pre-structured gold electrodes on the silicon substrate.

15.2.2.6.2 Liquid Crystal Reorientation

Polymer dispersed liquid crystals (PDLCs) consist of liquid crystal droplets randomly dispersed in a transparent polymer matrix. They are widely used in displays and optical elements, where the application of an electric field to the PDLCs readily adjusts the light transmittance through the material. In addition to PDLC realignment *via* an electric field, several reports have shown that liquid crystals can also be realigned using acoustics.[121] Recently, Liu *et al.* reported a light shutter effect induced by TSAWs applied to PDLCs.[122] As shown in Figure 15.11(a), PDLCs were placed between two IDTs on a $LiNbO_3$ substrate. In this setup, one IDT generated SAWs and the other detected them. Results demonstrated that SAW-induced acoustic streaming successfully aligned PDLCs parallel to the SAW propagation direction, changing the PDLCs from opaque to transparent (Figure 15.11(b)).

During experimentation, SAW propagation on the substrate heated the PDLCs to 40 °C. To verify that the PDLC realignment was attributable to SAW-induced acoustic streaming and not to thermal effects, the researchers set up an experiment using standing SAWs rather than TSAWs. This standing SAW field minimized the acoustic streaming effect while still heating the substrate and PDLCs; no PDLC realignment was observed. Therefore, the authors concluded that SAW-induced acoustic streaming is a viable actuation method for PDLC realignment.

Most recently, Liu *et al.* demonstrated the robustness of this effect by showing that application of a SAW field can also be used to control light transmission of holographic polymer-dispersed liquid crystals.[123]

15.2.3 Microfluidic Technologies Enabled by Phononic Crystal-assisted TSAWs

15.2.3.1 Introduction to Phononic Crystals

In the past decade, there has been a tremendous growth of interest in two- and three-dimensional periodic structures due to their ability to manipulate the propagation of acoustic waves on the wavelength scale. These artificial periodic structures, known as phononic crystals (PCs), are composed of

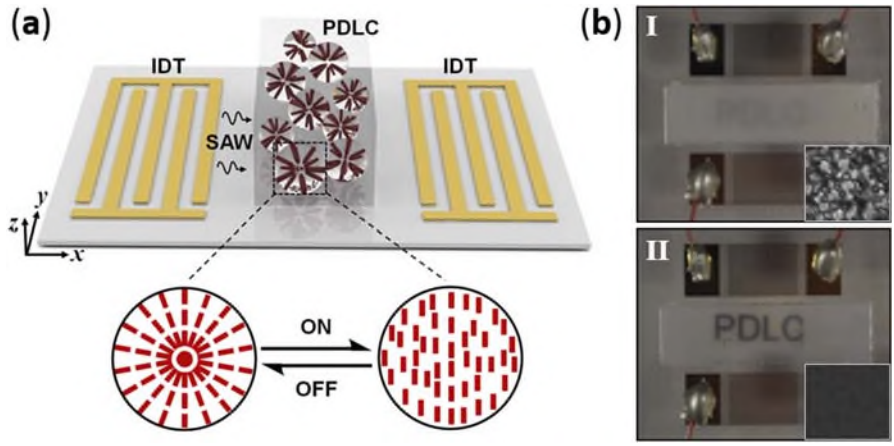

Figure 15.11 (a) The device structure and working principle for the SAW-driven PDLC light shutter. The magnified part shows a reversible switching process between two different liquid crystal droplet configurations. (b) Transmission response of the PDLCs under different acoustic powers. The insets I and II show the imaging quality at the off and on states of the IDT, respectively. Reprinted with permission from ref. 122.

arrays of elastic scatterers embedded in elastic host materials with properties different from those of the scatterers. PCs exhibit several unique behaviors as a result of their structures. Of greatest interest are so-called "phononic band gaps", which occur when phonon wavelengths correspond to the scale of the PC's periodicity. In phononic band gaps, acoustic waves in any vibration mode cannot penetrate the PC's structure in any direction due to destructive interference caused by phonon reflections from the periodic scatterers.[124,125]

The properties that result from PCs' periodic structure allow them to function in a wide variety of applications. The predictable responses produced by phononic band gaps make PCs promising candidates for perfect acoustic mirrors and for acoustic filters at designated frequencies. Likewise, PCs can serve as resonators and acoustic waveguides because any defect in a PC will contain acoustic wave vibrations when operating within the phononic band gap. Most importantly, PCs can be used to achieve super-resolution acoustic imaging when they exhibit negative refraction (the phenomenon occurring at the interface of materials in which acoustic waves are refracted opposite to the typically expected refraction).[126] Super-resolution acoustic imaging has been obtained because of the PC-based acoustic lens' ability to overcome the diffraction limit. Recently, with the introduction of a gradient-index (GRIN) concept to PC, a new class of PC was born. GRIN PC adds the ability to bend, focus, and modify the aperture of an acoustic beam to the already powerful capabilities of PCs.[127–131]

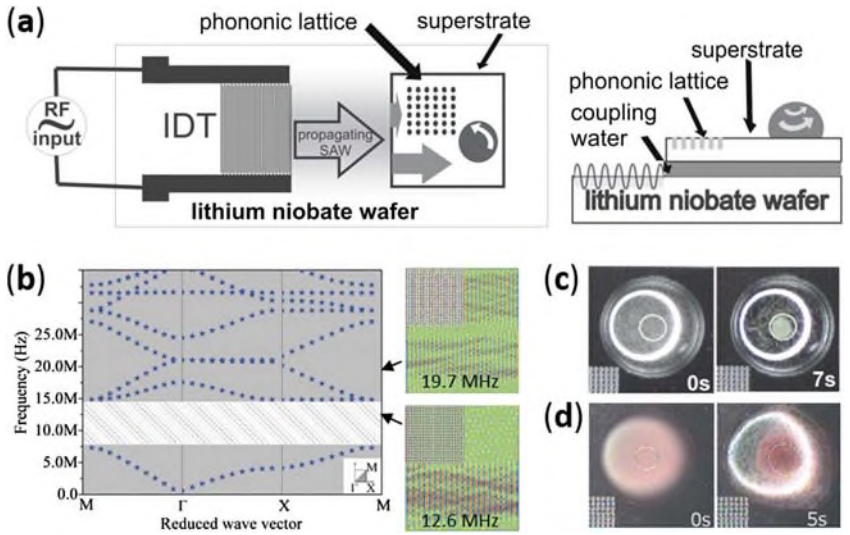

Figure 15.12 (a) Schematic of SAW device using a superstrate with embedded PC. TSAWs generated by IDT on the $LiNbO_3$ substrate leak into a water-coupling layer, inducing Lamb waves in the silicon superstrate that are then spatially filtered by the phononic lattice to provide asymmetric exposure to the droplet. (b) Left panel shows the band structure of the designed phononic lattice; the shaded area depicts the absolute phononic band gap. Right panel shows simulations at two different frequencies. (c) Concentration of 10 μm polystyrene beads at the center of the droplet due to circular acoustic streaming. (d) Concentration of human blood cells at the center of the droplet. Reprinted with permission from ref. 132.

PCs and GRIN PCs are considered the most promising candidates for solving low-frequency noise reduction issues and for providing ideal acoustic isolation for communication-band SAW devices. Moreover, the combination of PCs with SAW-based microfluidic devices can improve the performance of existing SAW microfluidic technologies and lead to novel applications. Though the field of PCs is still relatively new, it offers tremendous potential. In the following sections, we introduce a few examples of the successful technologies that arise from merging PCs with TSAWs.

15.2.3.2 Particle/Cell Concentration

To accomplish particle concentration in a droplet on the surface of a superstrate, Wilson *et al.* exploited the absolute phononic band gap of a PC.[132] As shown in Figure 15.12(a), an IDT was fabricated on a $LiNbO_3$ wafer to generate TSAWs. A PC consisting of circular holes in a square array was designed to exhibit a wide phononic band gap and fabricated on a silicon wafer (Figure 15.12(b)). When a SAW is generated at the proper frequency by

the IDT, it travels along the surface of the $LiNbO_3$ substrate, leaks into a water-coupling layer, and excites Lamb waves across the thickness of the silicon superstrate that propagate in the same direction as the SAWs. Half of the excited Lamb waves encounter and are reflected by the PC, and the other half travel through the superstrate undisturbed. Thus the water droplet experiences an asymmetric Lamb wave exposure, and an in-plane counter-clockwise acoustic streaming pattern is induced. Figure 15.12(c) shows the induced circular acoustic streaming being used to focus small particles inside a droplet. The Cooper group also used this method to concentrate human blood cells from a diluted blood sample, demonstrating its applicability in biology and medicine (Figure 15.12(d)).

Despite the added complexity to the manufacturing processes, the use of PCs in acoustic streaming applications enables some notable advantages. For example, PCs with different design characteristics can be used to tune the frequency and amplitude of a single SAW, allowing users to program fluid manipulation without altering the input electrical signal. In addition, PCs and IDTs can be fabricated independently on separate units (*e.g.*, substrates and superstrates, coupled by an intermediate fluid layer), enabling device configurability and disposability. Several studies have applied these advantages to create useful technologies. For example, Bourquin *et al.* combined droplet manipulation *via* acoustic streaming with a lens-free detection system to create a disposable device for immunoassay.[133] Applying their immunoassay to tuberculosis diagnosis, the researchers detected Interferon γ at pM concentrations within minutes. Reboud *et al.* developed a sophisticated SAW-based fluid manipulation tool for the detection of rodent malaria parasite *Plasmodium berghei* in blood.[134] Red blood cells and the parasitic *Plasmodium berghei* in a drop of blood were mechanically lysed *via* the strong acoustic rotation vortices generated by PC-aided acoustic streaming. The researchers then amplified the parasitic genomic sequence by heating the sample using different acoustic field and frequencies. Their results demonstrated that this PC-assisted device has the ability to detect around 0.07% parasite DNA in a microlitre-size blood sample and, more broadly, that it has potential for disease diagnosis in the developing world.

15.2.3.3 Jetting and Nebulization

Recently Bourquin *et al.* reported an interfacial jetting phenomenon by fabricating a conic PC on a superstrate.[135] Though jetting of a sessile droplet had been previously demonstrated using focused IDTs on a piezoelectric surface,[100] it had not been shown on a superstrate. In this work, the authors forced a SAW in a piezoelectric substrate to couple with a superstrate and excite Lamb waves (Figure 15.13(a)). The cone-shaped design of the PC they used provided a means to effectively focus acoustic energy to different hot spots, depending on the frequency of the SAW, as shown in Figure 15.13(b). They used this spatial control of acoustic energy to dictate the location and

direction of the interfacial jetting behavior; Figure 15.13(c) shows that this focused acoustic energy can efficiently produce an interfacial jetting phenomenon.

The researchers used a similar conical PC superstrate setup to selectively nebulize drops, as shown in Figure 15.13(d) and (e).[136] In Figure 15.13(d), a droplet was nebulized at position 3 when a SAW at 12.6 MHz excited the phononic structure. Meanwhile in Figure 15.13(e), a SAW frequency of 9.4 MHz caused the droplet nebulization to occur at position 1. This PC-assisted selective jetting and nebulization technology adds versatility to the applications of TSAWs and may be useful for the nebulization of drugs.

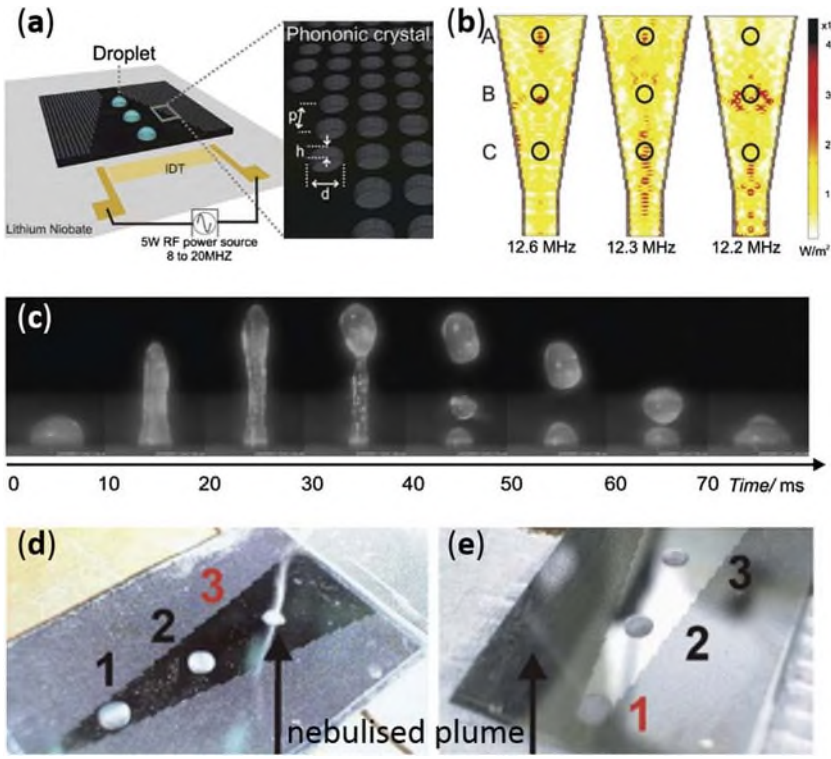

Figure 15.13 (a) Schematic of the SAW-induced interfacial jetting device. (b) Simulations of the conic structure at three different input frequencies. The waves are focused at different positions depending on the frequencies. (c) Continuous microscopic images of the jetting phenomenon on a PC superstrate for a sessile droplet of 10 μL. The drop elongates to form a column of water and breaks up into droplets. Images in (d) and (e) show, alternately, drops at position 3 (excited at 12.6 MHz) and position 1 (excited at 9.4 MHz) being selectively nebulized on the conic phononic superstrate (at a power of 3 W) while the other two drops remain. Reprinted with permission from refs. 135 and 136.

15.3 Standing Surface Acoustic Wave (SSAW) Microfluidics

15.3.1 Theory Involved with SSAW

The basic principles that govern the interference of all waves give rise to the formation of SSAWs.[137–144] If a pair of identical IDTs fabricated on a piezoelectric material generates two travelling SAWs propagating toward each other, the SAWs' interference will result in a one-dimensional SSAW field as shown in Figure 15.14(a). Computational analysis of a one-dimensional SSAW on the surface of a substrate has led to the simulated interference pattern shown in Figure 15.14(b). The light and dark regions represent weak and strong amplitudes of the sound pressure field, respectively. The lightest and darkest lines show that SSAWs have a series of nodes (minimum field) and anti-nodes (maximum field) at fixed locations on the substrate surface. The distance between neighboring nodes—and also the distance between neighboring anti-nodes—is always half of the SAW wavelength on the

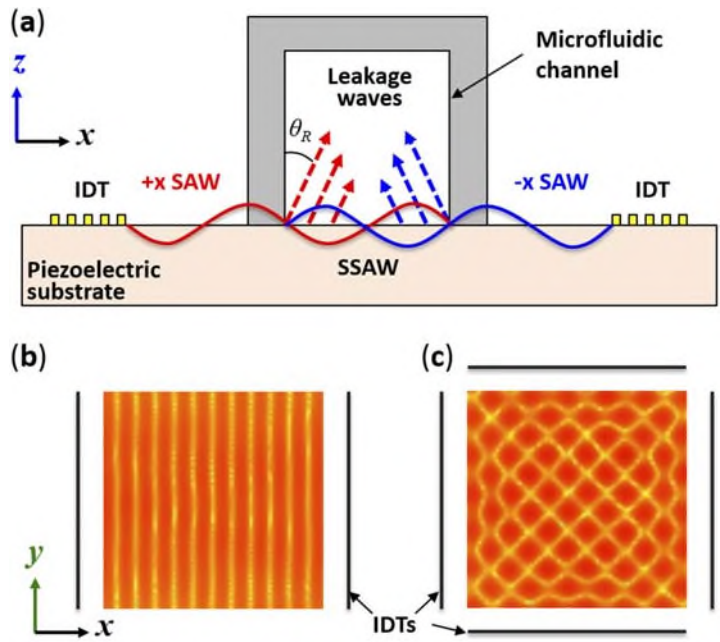

Figure 15.14 (a) A cross-section schematic of a microfluidic channel and the two IDTs used to generate travelling SAWs that propagate in opposite directions, establishing a SSAW across the channel width. This SSAW radiates acoustic leakage waves into the liquid at the Rayleigh angle. (b) and (c) show the simulated interference pattern of a one-dimensional and two-dimensional SSAW field on the substrate surface, respectively.

substrate. BAW-based approaches typically use acoustically reflective materials in channel walls to form standing waves within the channel (or cavity), which inherently gives a precise spatial definition of the standing wave pattern. In contrast, the SSAW-based approaches create standing waves through direct interference of two or more identical SAWs and do not require channel walls to be made of acoustically reflective materials. It should be noted that the phase of the two counter propagating waves has to be accurately controlled to ensure a fixed interference pattern over time.

Similar to the one-dimensional case, a two-dimensional SSAW field can be formed on the surface of a substrate by generating SAWs from two pairs of IDTs arranged orthogonally, as shown in Figure 15.14(c). Note that the two-dimensional interference pattern is tilted 45° with respect to the propagation direction of each SAW, and the shortest distance between nodes—and also the shortest distance between anti-nodes—in this two-dimensional patterned array is $\sqrt{2}/2$ times the SAW wavelength on the substrate.

SSAW-based microfluidic devices establish a standing acoustic field in fluid by means of IDT pairs forming a SSAW on a piezoelectric substrate in contact with the fluid (such as the setup in Figure 15.14(a)). As discussed in Section 15.3.1, we have good understanding of the SSAW field present on the piezoelectric substrate. However, if we are to explain the working mechanism of SSAW-based microfluidic devices, we must understand the standing acoustic field present in the fluid (as induced by acoustic energy leakage from the contacting substrate).

A recent study by Shi and colleagues[138] details a computational method used to model the SSAW-induced pressure field in the microfluidic channel depicted in Figure 15.14(a). The pressure gradient above the surface of the piezoelectric substrate leads to the generation of a longitudinal sound wave in the liquid. The displacement fields of the leakage wave created by two opposing travelling SAWs are plotted in Figure 15.15(a) and (b). Figure 15.15(c) and (d) show the pressure fields corresponding to the combined displacement fields at two time snapshots with half a period time difference. During the time between the two snapshots, the amplitude of the pressure in the vertical center of the channel remains zero (indicated by the dashed line in Figure 15.15(c) and (d)), while pressure in the other channel regions simply changes sign. These results indicate the existence of a standing acoustic pressure field in the fluid of the channel. Furthermore, the pressure nodal plane of this standing acoustic field sits immediately above the pressure node of the substrate SSAW that induced it. Several groups have experimentally confirmed the correspondence between pressure nodes of SSAW on the substrate and the acoustic field in the fluid.[139–143] The authors' computational model of the SSAW also demonstrated that the resulting primary acoustic radiation forces consist of axial mode (acting along the channel width) and transverse mode (acting along the channel height). The axial primary force is stronger than the transverse primary force. The partially reflected waves from the PDMS channel walls are included in the model to calculate the transverse primary force. For more details on SSAW theory, see Chapter 14.

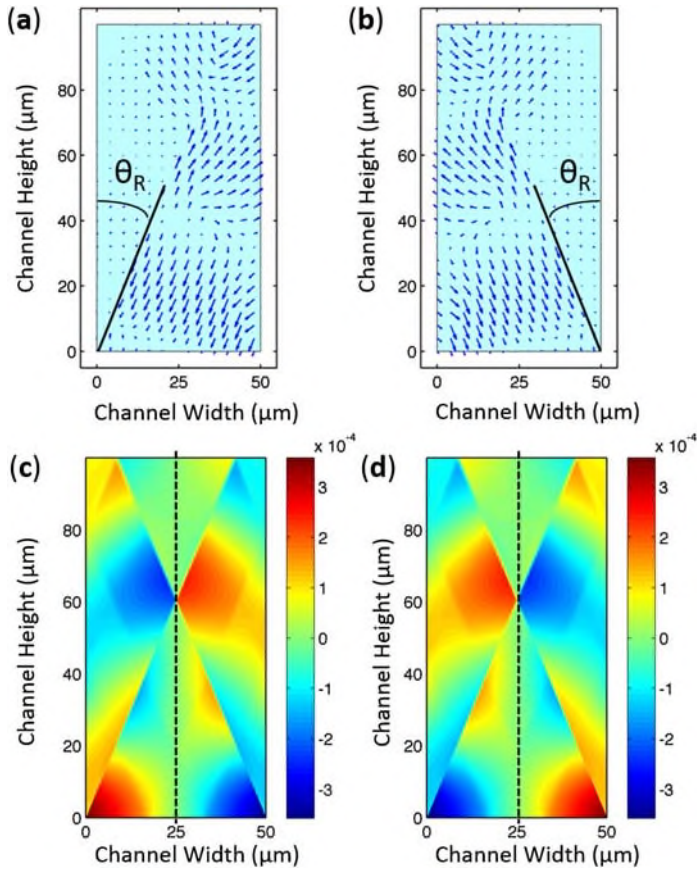

Figure 15.15 Time snapshots of the displacement field of the longitudinal-mode leakage wave from a SAW propagating in (a) the positive x-direction and (b) the negative x-direction. The width of the channel is half the SAW wavelength and the height is one SAW wavelength. The pressure field resulting from the combined displacement fields (*i.e.* resulting from a SSAW on the substrate) is shown in the cross-section of the channel at (c) $t = t_0$ and (d) $t = t_0 + \frac{\tau}{2}$ The dotted line denotes the pressure nodal plane in the middle of the channel. Reprinted with permission from ref. 138.

15.3.2 Microfluidic Technologies Enabled by SSAWs

Section 15.2.2 detailed the notable on-chip technologies and applications of TSAWs. These applications harnessed the acoustic streaming induced by the TSAWs to perform useful functions such as fluid mixing and cell sorting. In this section, we review the latest on-chip innovations enabled by SSAWs. Instead of harnessing the acoustic streaming, SSAW-based devices use the primary acoustic radiation forces acting on particles *via* the surrounding

fluid. We will detail devices that use these primary acoustic radiation forces to (1) focus a flow stream of particles into a single-file line, (2) separate a flow stream of particles based on particle properties, (3) actuate a single particle/cell moving with a flow stream, (4) pattern a group of particles in stagnant fluid, (5) manipulate a single particle/cell/organism in stagnant fluid, (6) manipulate proteins, and (7) align micro/nano materials. These technologies enrich the flexibility and functionality of SSAW-based, on-chip particle manipulation and will prove essential in building next-generation lab-on-a-chip systems.

15.3.2.1 Focusing of Particles in a Flow Stream

Microfluidic focusing of particles in a liquid flow stream has attracted attention mainly due to its direct applicability to on-chip flow cytometry.[145–149] To detect particles *via* flow cytometry, the particles need to be lined up single-file so they can each pass individually through a detection point. Many microfluidic devices have achieved particle focusing hydrodynamically, using sheath flows to align a particle stream single-file in the middle of a microfluidic channel. However, these sheath flows add substantial bulk to the microfluidic chip, increasing chip complexity and size. Sheath flow also introduces additional shear stress to the cells, which could affect cell viability and other functions. Therefore, a number of researchers have been investigating particle focusing methods that eschew sheath flows. Some of the best methods have harnessed SSAWs.

Shi *et al.* accomplished particle focusing in a microfluidic channel by situating the channel between two IDTs such that a SSAW was established across the channel width with a single pressure node that was located at the channel center.[139] When particles passed through the region of SSAW exposure, the acoustic radiation force pushed them to the center of the microfluidic channel width (*i.e.*, two-dimensional focusing), as shown in Figure 15.16. Following this original work on SSAW-based particle focusing, Zeng *et al.* reported that adding Bragg reflectors inside or outside of the IDTs enhanced particle focusing effects.[150] These SSAW-based, sheathless particle-focusing devices can be conveniently fabricated and operated.

Though focusing of particles within the channel width satisfies the needs of some applications, others require that particles be focused in both the channel width and height (*i.e.*, three-dimensional focusing). 3D focusing is especially important for flow cytometry applications, as fixing particle position along the channel height minimizes fluorescence variations caused by varying focal depths. Shi *et al.* showed that SSAW can effectively achieve 3D focusing.[138] Applying a SSAW to fluid in a microchannel, the researchers realized that a non-uniform acoustic field generates a primary acoustic radiation force transverse to the particles in the channel (*i.e.*, in the *z*-direction, relative to the device plane). This force will direct all of the particles towards the point of maximum acoustic kinetic energy. However, the acoustic radiation force acting in the *z*-direction is weaker than that acting in

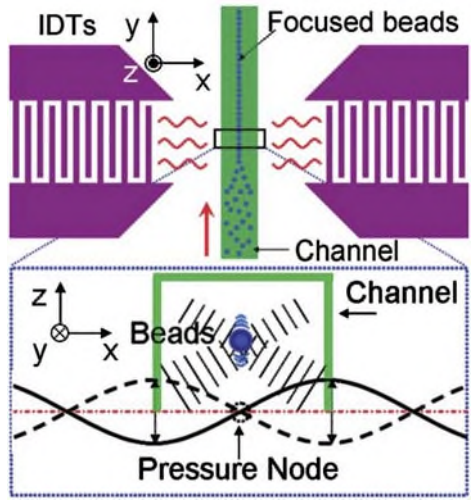

Figure 15.16 Schematic and working mechanism of SSAW-based focusing of particles in a liquid flow stream. Reprinted with permission from ref. 139.

the device plane. Therefore, particles focus first along the channel width and then migrate to a focal point along the channel height. The researchers used a prism placed adjacent to the microchannel to verify experimentally that particles did, in fact, focus in the *z*-direction; they then validated this with theoretical calculations.

15.3.2.2 Continuous Separation of Particles in a Flow Stream

A standing acoustic wave field exerts a primary acoustic radiation force whose magnitude and direction depend on particle size, density, and compressibility. Therefore, SSAW fields can differentiate particles or cells based on their physical properties. Shi *et al.* first reported SSAW-based continuous separation of particles in a flow stream in a PDMS microfluidic device.[151] The researchers situated a microfluidic channel between two IDTs such that a SSAW was established across the channel width with half a wavelength spanning the channel and a single pressure node at the channel center. The researchers introduced a particle mixture into the channel from side inlets while simultaneously injecting a sheath flow from the center inlet (Figure 15.17(a)). Because larger particles tend to experience larger primary acoustic radiation force, they migrate to the pressure node faster than smaller particles. Therefore, with appropriate length of the SSAW exposure region, SSAW enabled size-based particle separation. Larger particles move to the center outlet, while smaller particles remain in the side streams. This device demonstrated a simple, efficient, and cost-effective method for size-based particle separation.

Following the work of Shi *et al.*, Nam *et al.* developed a similar device setup and applied it to sorting blood cells from platelets.[152] First, to demonstrate the device, the researchers pumped a mixture of large and small particles through a separation channel from the device's center inlet while introducing sheath flows from side inlets. By positioning SSAW pressure nodes near the channel walls, the researchers managed to move larger particles from the center stream towards the channel sides. Smaller particles could then be collected from a middle outlet, while larger particles were collected from side outlets.

Nam *et al.* then applied this device setup to blood samples in order to separate platelets from red and white blood cells.[153] Because platelets are smaller than red and white blood cells, SSAW exposure in the separation channel resulted in large primary acoustic radiation forces pushing the red and white blood cells to the channel sides while platelets remained in the channel center. The SSAW-based sorting process effectively removed 99% of blood cells and achieved 74% separation efficiency for platelets. The work of Nam *et al.* demonstrated that SSAW not only effectively sorts particles, but also efficiently differentiates components of biological samples.

In addition to separating a particle flow stream based on particle size, SSAW devices can separate based on particle density. Cell-encompassing polymer beads provide one such example. There are numerous potential biological applications associated with encapsulating cells in biocompatible polymers. Although researchers have effectively generated mono dispersive polymer beads, they often struggle when attempting to control the number of cells encased by each polymer bead. To circumvent this challenge, Nam *et al.* exploited the increased polymer bead density associated with multiple contained cells. As a particle stream of polymer beads was flowed through a channel, the researchers used a SSAW with pressure nodes at either channel wall to drive the more dense beads to the channel sides while the less dense beads remained in the channel center.[154] In this device, large-cell-quantity alginate beads (LQABs), small-cell-quantity alginate beads (SQABs), and empty beads were collected from their respective outlets (Figure 15.17(b)). The device attained 97% separation efficiency and 98% separation specificity for LQABs. This device demonstrated that SSAWs can be employed to effectively sort particles in a flow stream based on both size and density.

Supplementing the work of previous groups, Jo *et al.* reported a sheathless method to separate equally-sized polystyrene and melamine beads based on their density differential.[155] To achieve sheathless separation, the researchers placed two pairs of IDTs side-by-side along a microfluidic channel. The first IDT pair generated a SSAW field with a pressure node in the channel center in order to focus the particle stream. After passing through the first IDT pair and being focused into a single-file line, the particle stream passed through the second IDT pair. The second IDT pair generated a SSAW field with pressure nodes at the channel walls, pushing the high-density melamine

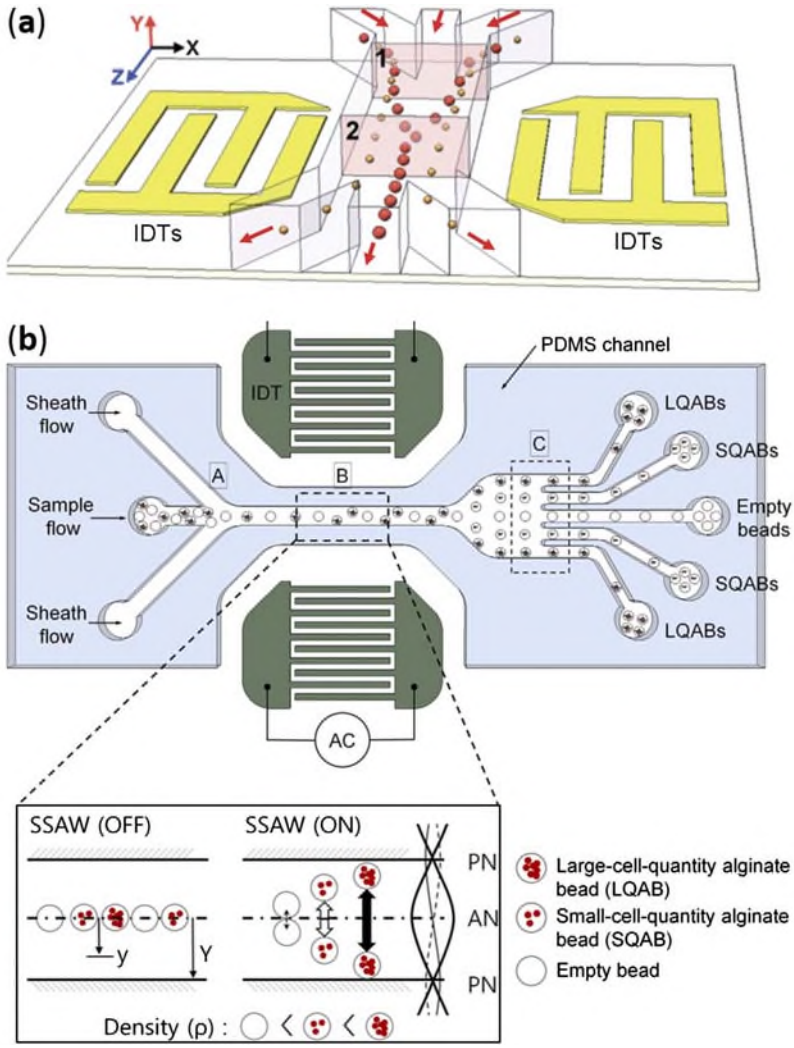

Figure 15.17 (a) Schematic of device for SSAW-based separation of particles in a liquid flow stream, based on particle size. (b) Schematic of device for SSAW-based separation of cell-encapsulating polymer beads in a liquid flow stream, based on bead density. Reprinted with permission from refs. 151 and 154.

beads (1.71 g cm^{-3}) to the channel sides while low-density polystyrene beads (1.05 g cm^{-3}) remained in the center stream. The device achieved 89.4% separation efficiency at a 2 μL min^{-1} flow rate, demonstrating the ability of SSAW to focus and separate particles all in one integrated unit. Guldiken *et al.* also reported an integration of SSAW-based focusing and separation to achieve sheathless separation of particles in a flow stream.[156]

15.3.2.3 Actuating a Single Particle in a Flow Stream

The previous section described how SSAW could be used to continuously separate a flow stream of particles based on the particles' physical properties (size and density). However, there are situations where it is desirable to sort a single particle moving in a liquid flow stream. A prime example is on-chip flow cytometry. After particles are focused and individually detected they are often sorted based on a property determined during detection (*e.g.*, presence of a cell surface protein as determined by fluorescence). Several mechanisms have been proposed for on-chip particle/cell actuation including electrokinetic, magnetic, optical, and hydrodynamic forces.[157–161] Recently, researchers have also proposed SSAW-based particle/cell actuation.[162–168]

While TSAW-based cell actuation (described in Section 15.2.2.5) utilizes acoustic streaming to move a cell, SSAW-based actuation moves the cell by means of primary acoustic radiation force. Because this primary acoustic radiation force pushes cells, particles, and droplets toward the SSAW pressure nodes (or anti-nodes, depending on their properties), these objects can be moved across the width of a microfluidic channel—and thereby sorted—by changing the position of a SSAW pressure node (or anti-node). By manipulating SSAW phase, researchers have demonstrated precise 1D actuation of microobjects in continuous flow.[162–164] Most recently, Ding *et al.* utilized SSAW-based actuation to construct a tunable device that precisely sorts single cells in a liquid flow stream into as many as five separate outlet channels (Figure 15.18).[165] In their work, the researchers positioned a microfluidic channel between two parallel chirped IDTs; these chirped IDTs operated in a wide frequency range, allowing them to generate a variety of SAW wavelengths. The width of the device channel was carefully selected so that only one pressure node could exist between the channel walls. The researchers tested their sorting device by pumping HL-60 cells through the channel. At frequency f_1 (9.8 MHz), the primary acoustic radiation force pushed the cell towards the SSAW field pressure node positioned at the topmost outlet channel (Figure 15.18(a)). Switching the input frequency to f_5 (10.9 MHz) shifted the pressure node downward and guided the cell to the lowest outlet channel (Figure 15.18(b)). Intermediate input frequencies f_2, f_3, and f_4 were used to guide the cell to the intermediate outlet channels. Figure 15.18(c) shows multichannel cell sorting, in which the device sorted cells contained in a liquid flow stream into five separate channels. This device demonstration shows the feasibility of SSAW-based actuation for the sorting of individual cells in on-chip flow cytometry. Li *et al.* recently applied the same principle to sort water-in-oil droplets into five separate outlets with a throughput of 222 droplets per seconds.[166]

15.3.2.4 Patterning a Group of Particles in Stagnant Fluid

Techniques that can non-invasively arrange particles or cells (contained in a stagnant fluid) into desired patterns are invaluable for many biomedical applications, including microarrays, tissue engineering, and regenerative

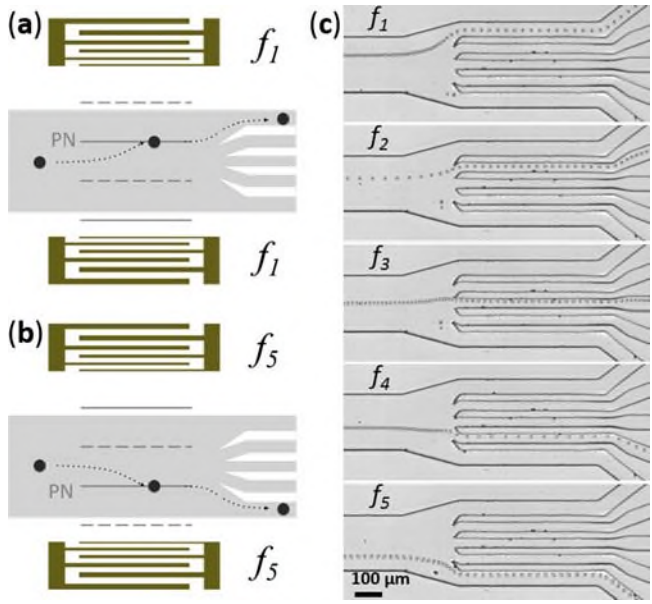

Figure 15.18 Left panel shows the working mechanism of SSAW-based sorting of a single cell contained in a liquid flow stream. (a) At an input signal frequency f_1 (9.8 MHz), the primary acoustic radiation force directs the cell to the pressure node at the upper wall of the channel, and the cell is collected from the topmost outlet. (b) At an input signal frequency f_2 (10.9 MHz), the pressure node is shifted to the lower wall of the channel, and the cell is collected from the lowermost outlet. Right panel (c) shows images of the experiment: HL-60 cells are driven individually to one of five desired outlet channels at five specific frequencies. Reprinted with permission from ref. 165.

medicine. The non-contact, non-invasive primary acoustic radiation forces generated by SSAWs serve as an excellent enabler of such particle/cell patterning techniques. Wood *et al.* exploited SSAWs to demonstrate the linear alignment of particles.[142] Following this work, Shi *et al.* developed "acoustic tweezers" to effectively and non-invasively arrange particles and cells.[141] The acoustic tweezers device consists of a PDMS microfluidic channel and a pair of IDTs deposited on a piezoelectric substrate in a parallel (Figure 15.19(a)) or orthogonal (Figure 15.19(b)) arrangement. After applying a RF signal to both IDTs to generate a SSAW field, particles/cells were patterned in parallel lines or arrays. Figure 15.19(c) and (d) show the distribution of microbeads before and after the 1D and 2D patterning processes. Patterning of massive particles in a large area has also been demonstrated using a similar mechanism and similar devices.[167]

The patterning of the aforementioned devices is static because the working frequency range of the SSAW is very narrow (the regular IDTs used in the devices have a bandwidth of ~0.2 MHz). In order to enable dynamic

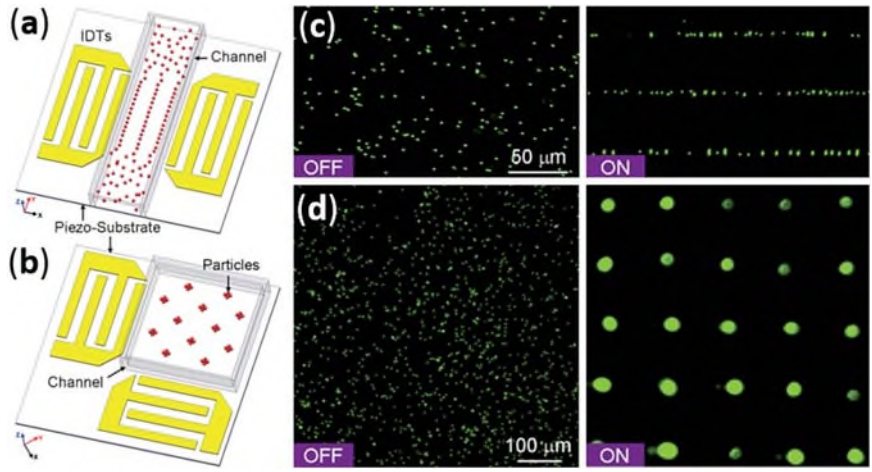

Figure 15.19 SSAW-based patterning of a group of particles in stagnant fluid. Schematic of (a) 1D patterning using two parallel IDTs, (b) 2D patterning using two orthogonal IDTs (the angle between the IDTs can be changed to achieve different patterns). (c) Distribution of fluorescent microbeads before and after the 1D (SAW wavelength was 100 um) patterning process, (d) and the 2D patterning process (SAW wavelength was 200 um). Reprinted with permission from ref. 141.

SSAW-based particle patterning, Ding *et al.* constructed a device with slanted-finger interdigital transducers (SFITs).[41] By tuning the input signal frequency, both the frequency and originating location of the main SAW beam can be tuned, permitting dynamic control of the particle patterning. The authors demonstrate SFIT-produced SSAW-based patterning of HL-60 leukemia cells; the period of the two cell lines was tuned to 60 μm, 78 μm, and 150 μm, using input signal frequencies of 45, 36, and 27 MHz, respectively.

15.3.2.5 Manipulating a Single Particle/Cell/Organism in Stagnant Fluid

In the previous section, we described recent developments in SSAW-based patterning for large numbers of particles/cells in stagnant fluid, with important biomedicine-related applications in microarrays, tissue engineering, and regenerative medicine. In addition to moving multiple particles/cell into a patterned formation, non-invasive manipulation of a single particle or cell contained in stagnant fluid is also invaluable in many biomedical applications, such as the study of cell-to-cell communication and interaction. Currently, many biologists employ optical tweezers for single-cell manipulation due to their excellent precision and versatility.[169] However, optical tweezers depend on complex and expensive optical setups, and the associated focused laser beam can heat the moved object to temperatures that cause

physiological damage. To reduce costs and minimize damage, researchers have been developing SSAW-based single-cell manipulation platforms.

When a single particle contained in stagnant fluid is exposed to a SSAW field, the primary acoustic radiation force acts on the particle and pushes it to either a pressure node or antinode (depending on the particle's properties), trapping it at that location. Once the particle has been trapped, it can be moved by changing the frequencies and phase of the constituent SAWs.[162–168] Ding *et al.* recently demonstrated SSAW-based manipulation on particles, cells, and even millimetre-sized *C. elegans* worms contained in stagnant fluid inside a microfluidic chamber.[29] Their device consisted of a 2.5×2.5 mm^2 PDMS chamber asymmetrically bonded to a $LiNbO_3$ substrate between two orthogonal pairs of chirped IDTs (Figure 15.20(a)). The two pairs of chirped IDTs allowed the device to move the objects trapped in the pressure nodes in the x and y directions independently. Figure 15.20(b) displays the effectiveness of this technique, as the researchers manipulated a single bovine red blood cell through a pre-programmed pattern, taking a photograph at each cell position and compositing the images to trace the cell's path. The researchers examined particle speed and potential for cell damage, finding that a 10 μm polystyrene bead is accelerated to a velocity as high as 1.6 mm s^{-1}, and that HeLa cells exhibited no significant physiological change after being exposed to high power acoustic fields for 10 min. Finally, the researchers placed *C. elegans* worms inside the chamber to show that they could move an entire organism without damage, as shown in Figure 15.20(c).

The acoustic tweezers device described above is biocompatible, versatile, low-cost, simple in design, and convenient to operate, making it an extremely attractive alternative to conventional optical tweezers for manipulation of single particles or cells. The successful trapping and manipulation of a whole organism also sets the device apart.

15.3.2.6 Protein Manipulation

Supported lipid bilayers (SLBs) are critically important in cellular biology, as they regulate the intracellular and intercellular movement of ions, proteins, and other molecules.[170] Recently, researchers have applied SSAWs to pattern SLBs for use in membrane biology studies. Hennig *et al.* showed that local concentrations of SLBs can be modulated by applying SSAW to a substrate.[171] In the experiment, standard IDTs generated shear SSAWs on a $LiTaO_3$ substrate to induce lateral reorganization of a lipid bilayer. Higher membrane density was found in the antinodes of the in-plane shear SSAW, while lower membrane density was found in the nodes. The researchers carefully monitored pattern formation and decay by fluorescence microscopy in order to study diffusion times of supported bilayers during the process. Diffusion times matched those attained with conventional methods, confirming the accuracy of SSAW for patterning of SLBs. Hennig *et al.* further demonstrated the modulation of DNA density on supported lipid bilayers by binding DNA to a catonic SLB.[172]

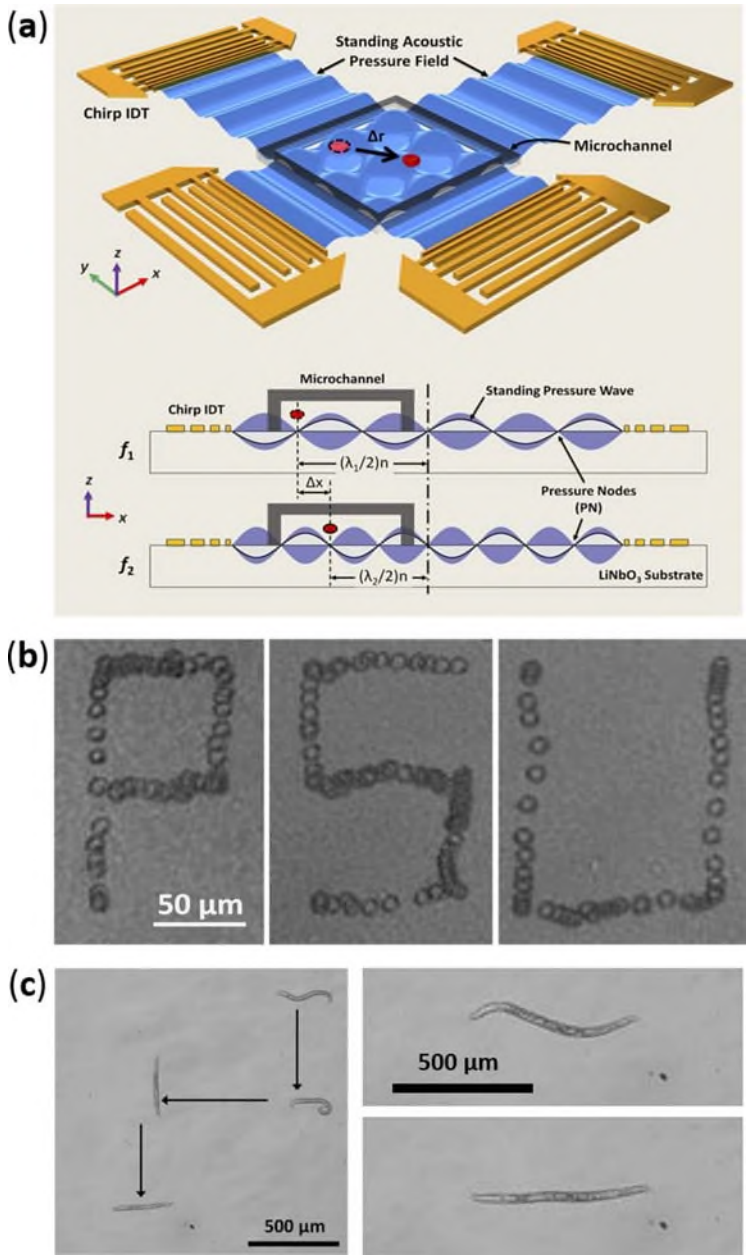

Figure 15.20 (a) Device schematic and working mechanism of SSAW-based manipulation of a single particle contained in stagnant fluid (*i.e.*, acoustic tweezers). (b) Composited image of a single bovine red blood cell translated in two dimensions by changing the frequencies of the constituent SAWs. (c) Optical images showing the manipulation and stretching of a whole *C. elegans* worm. Reprinted with permission from ref. 29.

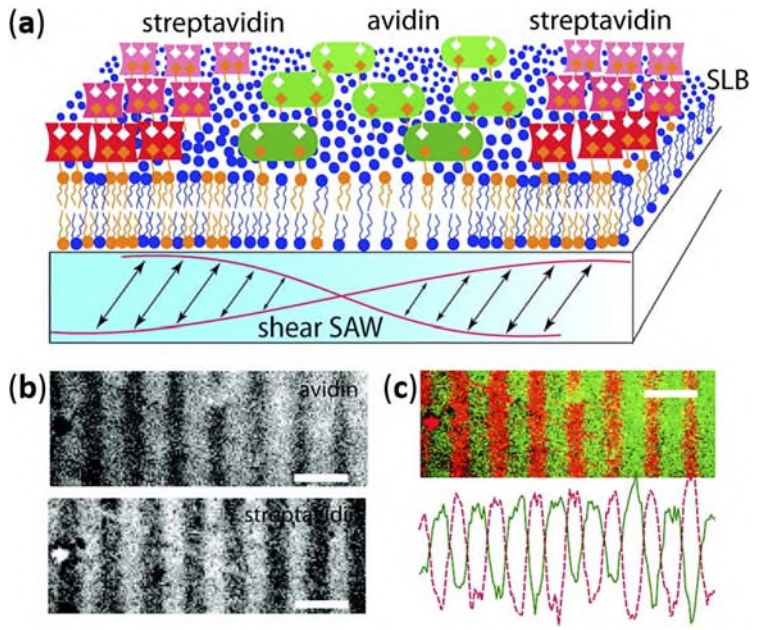

Figure 15.21 (a) Schematic of SSAW-based protein separation mechanism. A $LiTaO_3$ chip with IDTs (153 MHz/wavelength 26.6 μm) on opposite sides is used to generate a shear SSAW. The supported membrane (~4 nm thick) and protein segregation of membrane-bound streptavidin (red, Texas Red label) and avidin (green, Atto 488 label) can be observed by fluorescence microscopy through the optically transparent chip. (b) Fluorescence images of dye-labelled avidin and streptavidin. (c) Overlay images to demonstrate the segregation of avidin and streptavidin. Reprinted with permission from ref. 173.

Based on this lipid-patterning approach, Neumann *et al.* further demonstrated that proteins bound to SLBs can be accumulated, transported, and segregated using shear SSAWs.[173] As shown in recent work, SSAW-induced membrane modulations can achieve accumulation of labeled lipids. When the lipids are labeled with biotin, a biotin-binding protein called neutravidin accumulates alongside the lipids at pressure antinodes. The authors finely controlled the movement of proteins on SLBs by adjusting the phase between the two SAWs that combine to form the SSAWs. Phase adjustments in turn changed the locations of pressure nodes and antinodes, enabling protein transport in the 2D plane of the substrate. Finally, the group used shear SSAWs to separate avidin and streptavidin (two different biotin-binding proteins) based on their sizes (Figure 15.21(a)). Since streptavidin is the smaller of the two, it migrated towards the regions with high lipid bilayer densities at the antinodes. In contrast, SSAWs pushed the larger avidin proteins towards the pressure nodes, resulting in size-based protein segregation

(Figure 15.21(b)–(c)). Thus, SSAW-based microfluidic devices can be used to manipulate proteins on SLBs with operational simplicity and high success rate.

15.3.2.7 Microtube Alignment

In addition to using TSAWs to re-orientate micro/nano objects (see Section 15.2.2.6), researchers have also used SSAWs to align microtubes and nanowires.[174,175] Kong *et al.*[174] placed a droplet containing a suspension of rolled-up Cr microtubes on a $LiNbO_3$ substrate between two parallel IDTs. When the IDTs were energized and a SSAW was established in the substrate beneath the Cr microtube suspension, the microtubes uniformly aligned parallel to the propagation direction of the SAWs (Figure 15.22). In the SSAW field, these Cr tubes connected together end-to-end, forming tube bridges in a relatively high concentration.

To ascertain the physics underlying the alignment process, the researchers conducted control experiments with two sets of rolled-up microtubes, both conductive (Cr) and non-conductive (SiO/SiO_2), and two different piezoelectric surfaces, $LiNbO_3$ with a thin metal cover (to isolate the microtubes from the electric field at the substrate surface) and uncovered $LiNbO_3$ (exposing the microtubes to the electric field at the substrate surface). Experiment results showed that the Cr microtubes did not align on the metal-covered $LiNbO_3$ substrate, but did align on the uncovered $LiNbO_3$ substrate.

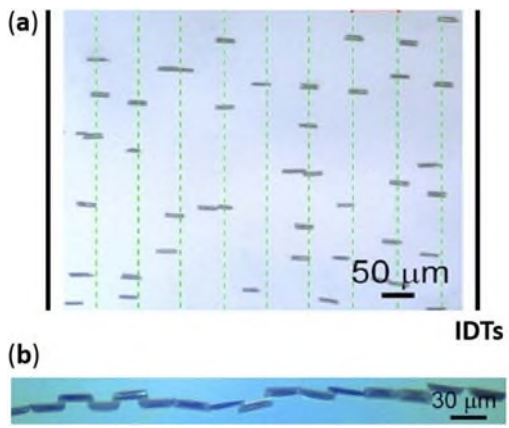

Figure 15.22 (a) Suspension of rolled-up Cr microtubes placed on a $LiNbO_3$ substrate between two parallel IDTs. IDTs are energized to establish a SSAW in the substrate, and the associated electric field uniformly aligned the microtubes parallel to the SAW propagation direction. (b) Optical image of aligned tube chain obtained from 30 μm long Cr tubes confined within the fluidic channel, after application of SAWs (30 MHz, 13 dBm). Reprinted with permission from ref. 174.

Furthermore, the SSAW exerted little influence on the non-conductive microtubes regardless of substrate. This proved that it was the electric field associated with the SSAW, and not the acoustic field, that was responsible for the alignment of the rolled-up metal microtubes.

15.4 Conclusions and Perspectives

As summarized in this book chapter, SAWs have demonstrated tremendous capability in microfluidic applications. TSAWs and SSAWs have, collectively, been used to achieve: rapid and localized fluid mixing, droplet translation, fluid pumping in microchannels, droplet-based rotational micromotors, droplet jetting and atomization, reorientation of nano-objects, as well as particle/cell focusing, sorting, manipulation, and patterning. Some of these functions have been achieved in microfluidics using techniques other than SAW as well. However, SAW has a combination of advantages that competing techniques lack: simple fabrication, high biocompatibility, versatility, compact and inexpensive devices and accessories, fast fluid actuation, contact-free particle manipulation, and compatibility with other microfluidic components. In addition, using SAW microfluidics, one can achieve functions that are unattainable by conventional methods. For example, non-invasive cell manipulation can be performed in a native cell environment, permitting normal cell growth and proliferation subsequent to the manipulation. This would have significant benefits in the study of stem cell differentiation, cell–cell communication, and tissue engineering. We believe that these unique advantages and functions position SAW to be a key component in the use of microfluidics as a tool in medical diagnostics and biological/chemical studies. For this to happen—for SAW microfluidic technologies to progress from research labs to everyday use in real-world applications—a number of hurdles must be overcome. In this section, we identify some of the areas requiring progress from both theorists and technical innovators.

The physics of SAW microfluidics, whether harnessing TSAW or SSAW, encompasses a range of phenomena, including acoustic radiation forces, acoustic streaming, jetting, and atomization. Theoretical work over the last two decades has fleshed out our understanding of this wide-ranging physics. However, work remains to be done if our theoretical understanding is to be complete. For instance, in the case of SAW-induced fluid atomization, there is an order of magnitude difference between the driving SAW frequency and the droplet excitation frequency (leading to atomization). This massive difference between driving and response frequencies remains poorly understood. Similarly, numerical simulations (*e.g.*, computational fluid dynamics modeling) of SAW-induced acoustic streaming have been hampered by the large discrepancy in the time and space domains between the driving SAW and the resulting liquid streaming. More specifically, a very small time step and a very fine mesh are required to capture the SAW actuation of the liquid, but the resulting streaming occurs over a relatively

large time scale and large spatial dimensions. Additionally, quantitative estimates of primary acoustic radiation force acting on complexly-shaped biological particles are currently inadequate, impeding the understanding and optimization of SSAW-based microfluidic platforms. Advancements in SAW-based microfluidic devices—and their adoption in real-world applications—will be strongly facilitated by SAW researchers improving the theoretical foundations of the discipline.

While the theorists do their part, there is much room for continued device innovations. As described throughout this chapter, much of SAW microfluidics to date has relied on either acoustic streaming or primary acoustic radiation forces to accomplish useful actions. These two phenomena occur simultaneously for both TSAW and SSAW, but for any given device application, the influence of one effect relative to the other is dictated by factors such as particle size, SAW type, SAW power, SAW frequency, and channel geometry.[176] For particle manipulation techniques that rely on SSAW, primary acoustic radiation forces are the enabler, and acoustic streaming is considered an undesirable concurrence that disrupts otherwise predictable particle movements. To improve the precision of SSAW-based particle manipulation, it would be beneficial for researchers to find ways to minimize acoustic. It should be pointed out that little research has been done on the acoustic streaming induced by SSAW. This is an area in need of attention; perhaps through some clever innovations, researchers may even be able to convert SSAW-induced acoustic streaming from a complicating factor to an enabling mechanism.

Further improvements to the exactness of SSAW-based particle manipulation are also needed. Current acoustic tweezers devices have micrometre-scale resolution. Their resolution could potentially be refined to the nanometre-scale by using high-frequency SAWs. However, increasing SAW frequency results in higher energy attenuation as the acoustic wave transfers from the substrate surface to the contacting fluid. High SAW frequencies also result in stronger acoustic streaming, which compounds the increasing effect of streaming on particle movement as the particle size decreases. Both the increased energy attenuation and augmented acoustic streaming will need to be addressed in order to improve the resolution, and thus the applicability, of SSAW-based particle manipulation.

In addition to the issue of manipulation resolution, researchers have struggled to achieve precise control of particle manipulation in the device out-of-plane (z) direction. Applications such as tissue engineering and cell–cell communications rely on careful control of cells in all three dimensions. For SSAW-based methods to become an all-around particle/cell manipulation solution, researchers will need to gain precise control of the z direction.

Other device innovations may come from the use of new piezoelectric substrates. Among the hundreds of piezoelectric materials, $LiNbO_3$ has found ubiquitous use in SAW microfluidics due to its transparency, which enables easy microscope observation of on-chip events. More effort could be applied to exploring the potential benefits of other substrate materials. For

example, the use of phononic crystals could help better manipulate SAW propagation and amplitude, and the use of piezoelectric thin films may lead to reduced device cost. In addition to considering new piezoelectric substrate materials, researchers should expand an existing trend: the use of disposable superstrates. These superstrates, which are bonded to the microfluidic components of the overall device, are acoustically coupled to the substrate *via* a liquid layer.[177,178] Such superstrates serve to separate the expensive piezoelectric substrate and its IDTs from the microfluidic components, making a single SAW-based device reusable by exchanging the superstrates. For example, if a cell patterning and culturing microfluidic device existed on a superstrate, multiple patterned superstrate cultures could be obtained with a single piezoelectric substrate. In combination with investigation of new substrate/superstrate materials, alternate acoustic modes, such as transverse SAW or plate waves, may also offer an opportunity for new innovations.

SAW-based microfluidics has come a long way in the past decade. It has been used to successfully perform a wide range of biomedicine-oriented lab functions, from cell focusing, cell sorting, cell manipulation, cell enrichment, cell lysis, to on-chip PCR, biosensing, and many more. In fact, these functions span the full spectrum of laboratory functions, from sample preparation all the way to final analysis; in other words, SAWs have been used to, on the aggregate, create a lab-on-a-chip. Researchers should now focus on actually creating that lab-on-a-chip. This will require integrating multiple SAW techniques onto a single microfluidic device, with transitions from one stage to another.

In order to make this adoption of SAW-based microfluidics a reality, researchers must build integrated devices capable of performing a complete conventional laboratory process, from start to finish. In this regard, facilitating the application of SAW-based microfluidics to real-world laboratory functions will take more than integrating multiple SAW techniques onto a coordinated device. It will also require creative solutions to a classic problem of microfluidic devices: the mismatch between coin-sized microchips and the large peripheral control and detection systems that still reside off-chip. Researchers will need to integrate function generators, amplifiers, SAW transducers, and signal processors onto a compact system. This integration and miniaturization is doable (SAW devices and accessories have already been integrated into compact, low-cost electronic devices such as cell phones), and it is necessary if SAW-based microfluidic devices are to be adopted for use in biological studies and medical diagnostics that researchers have long predicted.

Acknowledgements

This research was supported by the National Institutes of Health (1DP2OD007209-01) and the Penn State Center for Nanoscale Science (MRSEC) under grant DMR-0820404.

References

1. G. M. Whitesides, *Nature,* 2006, **442**, 368–373.
2. P. Neuzil, S. Giselbrecht, K. Länge, T. J. Huang and A. Manz, *Nat. Rev. Drug Discovery,* 2012, **11**, 620–632.
3. X. Mao and T. J. Huang, *Lab Chip,* 2012, **12**, 1412–1416.
4. M. L. Kovarik, D. M. Ornoff, A. T. Melvin, N. C. Dobes, Y. Wang, A. J. Dickinson, P. C. Gach, P. K. Shah and N. L. Allbritton, *Anal. Chem.,* 2013, **85**, 451–472.
5. T. M. Squires and S. R. Quake, *Rev. Mod. Phys.,* 2005, **77**, 977–1026.
6. A. Manz, N. Graber and H. M. Widmer, *Sens. Actuators, B,* 1990, **1**, 244–248.
7. A. Arora, G. Simone, G. Salieb-Beugelaar, J. T. Kim and A. Manz, *Anal. Chem.,* 2010, **82**, 4830–4847.
8. P. S. Dittrich and A. Manz, *Nat. Rev. Drug Discovery,* 2006, **5**, 210–218.
9. D. J. Beebe, G. A. Mensing and G. M. Walker, *Annu. Rev. Biomed. Eng.,* 2002, **4**, 261–286.
10. A. R. Wheeler, *Science,* 2008, **322**, 539–540.
11. I. A. Eydelnant, U. Uddayasankar, B. Li, M. W. Liao and A. R. Wheeler, *Lab Chip,* 2012, **12**, 750–757.
12. P. Tseng, J. W. Judy and D. D. Carlo, *Nat. Methods,* 2012, **9**, 1113–1119.
13. N. Pamme and A. Manz, *Anal. Chem.,* 2004, **76**, 7250–7256.
14. A. Lenshof and T. Laurell, *Chem. Soc. Rev.,* 2010, **39**, 1203–1217.
15. C. Monat, P. Domachuk and B. J. Eggleton, *Nat. Photonics,* 2007, **1**, 106–114.
16. X. Mao, J. R. Waldeisen, B. K. Juluri and T. J. Huang, *Lab Chip,* 2007, **7**, 1303–1308.
17. H. Schmidt and A. R. Hawkins, *Nat. Photonics,* 2011, **5**, 598–604.
18. Y. Zhao, Z. S. Stratton, F. Guo, M. I. Lapsley, C. Y. Chan, S.-C. S. Lin and T. J. Huang, *Lab Chip,* 2013, **13**, 17–24.
19. D. Psaltis, S. R. Quake and C. Yang, *Nature,* 2006, **442**, 381–386.
20. C. C. W. Ruppel, L. Reindl and R. Weigel, *Microwave Magazine,* 2002, **3**, 65–71.
21. A. Polh, *IEEE Trans. Sonics Ultrason.,* 2000, **47**, 317–332.
22. T. M. Gronewold, *Anal. Chim. Acta,* 2007, **603**, 119–128.
23. K. Länge, G. Blaess, A. Voigt, R. Götzen and M. Rapp, *Biosens. Bioelectron.,* 2006, **22**, 227–232.
24. A. Renaudin, V. Chabot, E. Grondin, V. Aimez and P. G. Charette, *Lab Chip,* 2010, **10**, 111–115.
25. J. Lee, Y.-S. Choi, Y. Lee, H. J. Lee, J. N. Lee, S. K. Kim, K. Y. Han, E. C. Cho, J. C. Park and S. S. Lee, *Anal. Chem.,* 2011, **83**, 8629–8635.
26. S.-C. S. Lin, X. Mao and T. J. Huang, *Lab Chip,* 2012, **12**, 2766–2770.
27. D. L. Miller, N. B. Smith, M. R. Bailey, G. J. Czarnota, K. Hynynen and I. R. S. Makin, *J. Ultrasound Med.,* 2012, **31**, 623–634.
28. M. Wiklund, *Lab Chip,* 2012, **12**, 2018–2028.
29. X. Ding, S.-C. S. Lin, B. Kiraly, H. Yue, S. Li, I. K. Chiang, J. Shi, S. J. Benkovic and T. J. Huang, *Proc. Natl. Acad. Sci. U. S. A.,* 2012, **109**, 11105–11109.

30. H. Li, J. Friend, L. Yeo, A. Dasvarma and K. Traianedes, *Biomicrofluidics,* 2009, **3**, 34102.
31. J. Friend and L. Y. Yeo, *Rev. Mod. Phys.,* 2011, **83**, 647–704.
32. L. Y. Yeo and J. R. Friend, *Biomicrofluidics,* 2009, **3**, 012002.
33. H. Bruus, J. Dual, J. Hawkes, M. Hill, T. Laurell, J. Nilsson, S. Radel, S. Sadhal and M. Wiklund, *Lab Chip,* 2011, **11**, 3579–3580.
34. A. Wixforth, *J. Lab. Automat.,* 2006, **11**, 399–405.
35. D. Beyssen, L. Le Brizoual, O. Elmazria and P. Alnot, *Sens. Actuators, B,* 2006, **118**, 380–385.
36. X. Ding, P. Li, S.-C. S. Lin, Z. S. Stratton, N. Nama, F. Guo, D. Slotcavage, X. Mao, J. Shi, F. Costanzo and T. J. Huang, *Lab Chip,* 2013, **13**, 3626–3649.
37. Z. Wang and J. Zhe, *Lab Chip,* 2011, **11**, 1280–1285.
38. M. Gedge and M. Hill, *Lab Chip,* 2012, **12**, 2998–3007.
39. Y. Q. Fu, J. K. Luo, X. Y. Du, A. J. Flewitt, Y. Li, G. H. Markx, A. J. Walton and W. I. Milne, *Sens. Actuators, B,* 2010, **143**, 606–619.
40. M. K. Tan, J. R. Friend and L. Y. Yeo, *Appl. Phys. Lett.,* 2007, **91**, 224101.
41. X. Ding, J. Shi, S.-C. S. Lin, S. Yazdi, B. Kiraly and T. J. Huang, *Lab Chip,* 2012, **12**, 2491–2497.
42. K. Hashimoto and M. Yamaguchi, *IEEE Trans. Sonics Ultrason.,* 2001, **48**, 1181–1188.
43. C. T. Schröder and W. R. Scott Jr, *J. Acoust. Soc. Am.,* 2001, **110**, 2867–2877.
44. E. Adler, *IEEE Trans. Sonics Ultrason.,* 1994, **41**, 876–882.
45. B. Auld, *Acoustic Fields and Waves in Solids*, Wiley Press, New York, 1973.
46. D. Köster, *SIAM J. Sci. Comput.,* 2007, **29**, 2352–2380.
47. L. Meng, F. Cai, Q. Jin, L. Niu, C. Jiang, Z. Wang, J. Wu and H. Zheng, *Sens. Actuators, B,* 2011, **160**, 1599–1605.
48. M. Wiklund, R. Green and M. Ohlin, *Lab Chip,* 2012, **12**, 2438–2451.
49. A. Wixforth, C. Strobl, C. Gauer, A. Toegl, J. Scriba and Z. V. Guttenberg, *Anal. Bioanal. Chem.,* 2004, **379**, 982–991.
50. Q. Zeng, F. Guo, L. Yao, H. W. Zhu, L. Zheng, Z. X. Guo, W. Liu, Y. Chen, S. S. Guo and X. Z. Zhao, *Sens. Actuators, B,* 2011, **160**, 1552–1556.
51. J. Vanneste and O. Buhler, *Proc. R. Soc. London, Ser. A,* 2010, **467**, 1779–1800.
52. M. Alghane, B. X. Chen, Y. Q. Fu, Y. Li, J. K. Luo and A. J. Walton, *J. Micromech. Microeng.,* 2011, **21**, 015005.
53. X. Y. Du, Y. Q. Fu, J. K. Luo, A. J. Flewitt and W. I. Milne, *J. Appl. Phys.,* 2009, **105**, 024508.
54. W.-K. Tseng, J.-L. Lin, W.-C. Sung, S.-H. Chen and G.-B. Lee, *J. Micromech. Microeng.,* 2006, **16**, 539–548.
55. T. Frommelt, D. Gogel, M. Kostur, P. Talkner, P. Hänggi and A. Wixforth, *IEEE Trans. Sonics Ultrason.,* 2008, **55**, 2298–2305.
56. R. Shilton, M. K. Tan, L. Y. Yeo and J. R. Friend, *J. Appl. Phys.,* 2008, **104**, 014910.
57. D. Köster, PhD Thesis, Augsburg University, 2006.

58. W. L. Nyborg, in *Acoustic Streaming*, ed. W. P.Mason and R. N.Thurston, Academic Press, New York, 1965, vol. 11, pp. 265–329.
59. S. S. Sadhal, *Lab Chip,* 2012, **12**, 2292–2300.
60. C. Bradley, *J. Acoust. Soc. Am.,* 1996, **100**, 1399–1408.
61. H. Bruus, *Lab Chip,* 2012, **12**, 20–28.
62. L. Zarembo, in *Acoustic Streaming*, Plenum Press, New York, 1971, pt. III, pp. 138–199.
63. A. A. Doinikov, *J. Fluid Mech.,* 1994, **267**, 1–21.
64. F. Costanzo, G. L. Gray and P. C. Andia, *Int. J. Eng. Sci.,* 2005, **43**(7), 533–555.
65. P. C. Andia, F. Costanzo and G. L. Gray, *Int. J. Solids Struct.,* 2005, **42**, 6409–6432.
66. L. V. King, *Proc. R. Soc. London, Ser. A,* 1934, **147**, 212–240.
67. K. Yosioka and Y. Kawasima, *Acustica,* 1955, **5**, 167–173.
68. L. P. Gorkov, *Sov. Phys. Dokl.,* 1962, **6**, 773–775.
69. J. Dual, P. Hahn, I. Leibacher, D. Moller, T. Schwarz and J. Wang, *Lab Chip,* 2012, **12**, 4010–4021.
70. H. Bruus, *Lab Chip,* 2012, **12**, 1014–1021.
71. M. Evander and J. Nilsson, *Lab Chip,* 2012, **12**, 4667–4676.
72. R. Barnkob, P. Augustsson, T. Laurell and H. Bruus, *Phys. Rev. E,* 2012, **86**, 056307.
73. T. Frommelt, M. Kostur, M. Wenzel-Schäfer, P. Talkner, P. Hänggi and A. Wixforth, *Phys. Rev. Lett.,* 2008, **100**, 034502.
74. T.-D. Luong, V.-N. Phan and N.-T. Nguyen, *Microfluid. Nanofluid.,* 2011, **10**, 619–625.
75. A. R. Rezk, A. Qi, J. R. Friend, W. H. Li and L. Y. Yeo, *Lab Chip,* 2012, **12**, 773–779.
76. A. Renaudin, P. Tabourier, V. Zhang, J. C. Camart and C. Druon, *Sens. Actuators, B,* 2006, **113**, 389–397.
77. T. A. Franke and A. Wixforth, *ChemPhysChem,* 2008, **9**, 2140–2156.
78. A. Wixforth, *Superlattices Microstruct.,* 2003, **33**, 389–396.
79. Z. Guttenberg, H. Muller, H. Habermüller, A. Geisbauer, J. Pipper, J. Felbel, M. Kielpinski, J. Scriba and A. Wixforth, *Lab Chip,* 2005, **5**, 308–317.
80. M. K. Tan, J. R. Friend and L. Y. Yeo, *Lab Chip,* 2007, **7**, 618–625.
81. H. Li, J. R. Friend and L. Y. Yeo, *Biomaterials,* 2007, **28**, 4098–4104.
82. A. R. Rezk, O. Manor, J. R. Friend and L. Y. Yeo, *Nat. Commun.,* 2012, **3**, 1167.
83. L. Schmid, A. Wixforth, D. A. Weitz and T. Franke, *Microfluid. Nanofluid.,* 2011, **12**, 229–235.
84. S. W. Schneider, S. Nuschele, A. Wixforth, C. Gorzelanny, A. Alexander-Katz, R. R. Netz and M. F. Schneider, *Proc. Natl. Acad. Sci. U. S. A.,* 2007, **104**, 7899–7903.
85. L. Masini, M. Cecchini, S. Girardo, R. Cingolani, D. Pisignano and F. Beltram, *Lab Chip,* 2010, **10**, 1997–2000.
86. M. Cecchini, S. Girardo, D. Pisignano, R. Cingolani and F. Beltram, *Appl. Phys. Lett.,* 2008, **92**, 104103.

87. S. Girardo, M. Cecchini, F. Beltram, R. Cingolani and D. Pisignano, *Lab Chip,* 2008, **8**, 1557–1563.
88. M. A. Fallah, V. M. Myles, T. Krüger, K. Sritharan, A. Wixforth, F. Varnik, S. W. Schneider and M. F. Schneider, *Biomicrofluidics,* 2010, **4**, 1–10.
89. C. Fillafer, G. Ratzinger, J. Neumann, Z. Guttenberg, S. Dissauer, I. K. Lichtscheidl, M. Wirth, F. Gabor and M. F. Schneider, *Lab Chip,* 2009, **9**, 2782–2788.
90. R. J. Shilton, N. R. Glass, P. Chan, L. Y. Yeo and J. R. Friend, *Appl. Phys. Lett.,* 2011, **98**, 254103.
91. R. J. Shilton, S. M. Langelier, J. R. Friend and L. Y. Yeo, *Appl. Phys. Lett.,* 2012, **100**, 033503.
92. N. R. Glass, R. J. Shilton, P. Chan, J. R. Friend and L. Y. Yeo, *Small,* 2012, **8**, 1881–1888.
93. J. Eggers, *Rev. Mod. Phys.,* 1997, **69**, 865–929.
94. P. Calvert, *Chem. Mater.,* 2001, **13**, 3299–3305.
95. B.-J. de Gans, P. C. Duineveld and U. S. Schubert, *Adv. Mater.,* 2004, **16**, 203–213.
96. M. K. Tan, J. R. Friend and L. Y. Yeo, *Phys. Rev. Lett.,* 2009, **103**, 024501.
97. A. Lefebvre, *Atomization and Sprays*, CRC Press, New York, 1989.
98. M. Kurosawa, T. Watanabe, A. Futami and T. Higuchi, *Sens. Actuators, A,* 1995, **50**, 69–74.
99. A. Qi, L. Y. Yeo, J. R. Friend and J. Ho, *Lab Chip,* 2010, **10**, 470–476.
100. A. Qi, J. R. Friend, L. Y. Yeo, D. A. V. Morton, M. P. McIntosh and L. Spiccia, *Lab Chip,* 2009, **9**, 2184–2193.
101. S. R. Heron, R. Wilson, S. A. Shaffer, D. R. Goodlett and J. M. Cooper, *Anal. Chem.,* 2010, **82**, 3985–3989.
102. S. H. Yoon, Y. Huang, J. S. Edgar, Y. S. Ting, S. R. Heron, Y. Kao, Y. Li, C. D. Masselon, R. K. Ernst and D. R. Goodlett, *Anal. Chem.,* 2012, **84**, 6530–6537.
103. A. Qi, P. Chan, J. Ho, A. Rajapaksa, J. Friend and L. Y. Yeo, *ACS Nano,* 2011, **5**, 9583–9591.
104. J. Ho, M. K. Tan, D. Go, L. Y. Yeo, J. Friend and H. C. Chang, *Anal. Chem.,* 2011, **83**, 3260–3266.
105. M. Alvarez, J. Friend and L. Y. Yeo, *Nanotechnology,* 2008, **19**, 455103.
106. J. R. Friend, L. Y. Yeo, D. R. Arifin and A. Mechler, *Nanotechnology,* 2008, **19**, 145301.
107. O. V. Abramov, *High-Intensity Ultrasonics*, Gordon and Breach Science Publishers, Amsterdam, 1998.
108. L. Dong, A. Chaudhury and M. K. Chaudhury, *Eur. Phys. J. E: Soft Matter Biol. Phys.,* 2006, **21**, 231–242.
109. M. K. Tan, J. R. Friend, O. K. Mata and L. Y. Yeo, *Phys. Fluids,* 2010, **22**, 112112.
110. D. J. Collins, O. Manor, A. Winkler, H. Schmidt, J. R. Friend and L. Y. Yeo, *Phys. Rev. E,* 2012, **86**, 056312.
111. H. Li, J. R. Friend and L. Y. Yeo, *Biomed. Microdevices,* 2007, **9**, 647–656.
112. P. R. Rogers, J. R. Friend and L. Y. Yeo, *Lab Chip,* 2010, **10**, 2979–2985.

113. M. K. Tan, J. R. Friend and L. Y. Yeo, *Lab Chip,* 2007, **7**, 618–625.
114. T. Franke, A. R. Abate, D. A. Weitz and A. Wixforth, *Lab Chip,* 2009, **9**, 2625–2627.
115. T. Franke, S. Braunmüller, L. Schmid, A. Wixforth and D. A. Weitz, *Lab Chip,* 2010, **10**, 789–794.
116. L. Schmid and T. Franke, *Lab Chip*, 2013, DOI: 10.1039/C3LC41233D.
117. R. H. Baughman, A. A. Zakhidov and W. A. de Heer, *Science,* 2002, **297**, 787–792.
118. C. J. Strobl, C. Schäflein, U. Beierlein, J. Ebbecke and A. Wixforth, *Appl. Phys. Lett.,* 2004, **85**, 1427–1429.
119. T. Smorodin, U. Beierlein, J. Ebbecke and A. Wixforth, *Small,* 2005, **1**, 1188–1190.
120. K. M. Seemann, J. Ebbecke and A. Wixforth, *Nanotechnology,* 2006, **17**, 4529–4532.
121. A. P. Malanoski, V. A. Greanya, B. T. Weslowski, M. S. Spector, J. V. Selinger and R. Shashidhar, *Phys. Rev. E,* 2004, **69**, 021705.
122. Y. J. Liu, X. Ding, S.-C. S. Lin, J. Shi, I.-K. Chiang and T. J. Huang, *Adv. Mater.,* 2011, **23**, 1656–1659.
123. Y. J. Liu, M. Lu, X. Ding, E. S. P. Leong, S.-C. S. Lin, J. Shi, J. H. Teng, L. Wang, T. J. Bunning and T. J. Huang, *J. Lab. Automat.*, 2012, doi: 10.1177/2211068212455632.
124. T.-T. Wu, Z.-G. Huang and S. Lin, *Phys. Rev. B,* 2004, **69**, 1–10.
125. S.-C. S. Lin and T. Huang, *Phys. Rev. B,* 2011, **83**, 174303.
126. J. Shi, S.-C. S. Lin and T. J. Huang, *Appl. Phys. Lett.,* 2008, **92**, 111901.
127. S.-C. Lin, T. Huang, J.-H. Sun and T.-T. Wu, *Phys. Rev. B,* 2009, **79**, 094302.
128. S.-C. S. Lin and T. J. Huang, *J. Appl. Phys.,* 2009, **106**, 053529.
129. S.-C. S. Lin, B. R. Tittmann, J.-H. Sun, T.-T. Wu and T. J. Huang, *J. Phys. D: Appl. Phys.,* 2009, **42**, 185502.
130. T.-T. Wu, Y.-T. Chen, J.-H. Sun, S.-C. S. Lin and T. J. Huang, *Appl. Phys. Lett.,* 2011, **98**, 171911.
131. S.-C. S. Lin, B. R. Tittmann and T. J. Huang, *J. Appl. Phys.,* 2012, **111**, 123510.
132. R. Wilson, J. Reboud, Y. Bourquin, S. L. Neale, Y. Zhang and J. Cooper, *Lab Chip,* 2010, **11**, 323–328.
133. Y. Bourquin, J. Reboud, R. Wilson, Y. Zhang and J. M. Cooper, *Lab Chip,* 2011, **11**, 2725–2730.
134. J. Reboud, Y. Bourquin, R. Wilson, G. S. Pall, M. Jiwaji, A. R. Pitt, A. Graham, A. P. Waters and J. M. Cooper, *Proc. Natl. Acad. Sci. U. S. A.,* 2012, **109**, 15162–15167.
135. Y. Bourquin, R. Wilson, Y. Zhang, J. Reboud and J. M. Cooper, *Adv. Mater.,* 2011, **23**, 1458–1462.
136. J. Reboud, R. Wilson, Y. Zhang, M. H. Ismail, Y. Bourquin and J. M. Cooper, *Lab Chip,* 2012, **12**, 1268–1273.
137. D. Hartono, Y. Liu, P. L. Tan, X. Y. S. Then, L.-Y. L. Yung and K.-M. Lim, *Lab Chip,* 2011, **11**, 4072–4080.

138. J. Shi, S. Yazdi, S.-C. S. Lin, X. Ding, I.-K. Chiang, K. Sharp and T. J. Huang, *Lab Chip,* 2011, **11**, 2319–2324.
139. J. Shi, X. Mao, D. Ahmed, A. Colletti and T. J. Huang, *Lab Chip,* 2008, **8**, 221–223.
140. M. Alvarez, J. R. Friend and L. Y. Yeo, *Langmuir,* 2008, **24**, 10629–10632.
141. J. Shi, D. Ahmed, X. Mao, S.-C. S. Lin, A. Lawit and T. J. Huang, *Lab Chip,* 2009, **9**, 2890–2895.
142. C. D. Wood, S. D. Evans, J. E. Cunningham, R. O'Rorke, C. Wälti and A. G. Davies, *Appl. Phys. Lett.,* 2008, **92**, 044104.
143. L. Johansson, J. Enlund, S. Johansson, I. Katardjiev and V. Yantchev, *Biomed. Microdevices,* 2012, **14**, 1–11.
144. L. Johansson, J. Enlund, S. Johansson, I. Katardjiev, M. Wiklund and V. Yantchev, *J. Micromech. Microeng.,* 2012, **22**, 025018.
145. M. E. Piyasena, P. P. A. Suthanthiraraj, R. W. Applegate, A. M. Goumas, T. A. Woods, G. P. López and S. W. Graves, *Anal. Chem.,* 2012, **84**, 1831–1839.
146. X. Mao, S.-C. S. Lin, C. Dong and T. J. Huang, *Lab Chip,* 2009, **9**, 1583–1589.
147. X. Mao, J. R. Waldeisen and T. J. Huang, *Lab Chip,* 2007, **7**, 1260–1262.
148. X. Mao, A. A. Nawaz, S.-C. S. Lin, M. I. Lapsley, Y. Zhao, J. P. McCoy, W. S. El-Deiry and T. J. Huang, *Biomicrofluidics,* 2012, **6**, 024113.
149. M. I. Lapsley, L. Wang and T. J. Huang, *Biomarkers Med.,* 2013, **7**, 75–78.
150. Q. Zeng, H. W. L. Chan, X. Z. Zhao and Y. Chen, *Microelectron. Eng.,* 2010, **87**, 1204–1206.
151. J. Shi, H. Huang, Z. Stratton, Y. Huang and T. J. Huang, *Lab Chip,* 2009, **9**, 3354–3359.
152. J. Nam, Y. Lee and S. Shin, *Microfluid. Nanofluid.,* 2011, **11**, 317–326.
153. J. Nam, H. Lim, D. Kim and S. Shin, *Lab Chip,* 2011, **11**, 3361.
154. J. Nam, H. Lim, C. Kim, J. Y. Kang and S. Shin, *Biomicrofluidics,* 2012, **6**, 024120.
155. M. C. Jo and R. Guldiken, *Sens. Actuators, A,* 2012, **187**, 22–28.
156. R. Guldiken, M. C. Jo, N. Gallant, U. Demirci and J. Zhe, *Sensors,* 2012, **12**, 905–922.
157. A. Y. Fu, C. Spence, A. Scherer, F. H. Arnold and S. R. Quake, *Nat. Biotechnol.,* 1999, **17**, 1109–1111.
158. F. Shen, H. Hwang, Y. K. Hahn and J.-K. Park, *Anal. Chem.,* 2012, **84**, 3075–3081.
159. A. J. Mach, O. B. Adeyiga and D. D. Carlo, *Lab Chip,* 2013, **13**, 1011–1026.
160. M. M. Wang, E. Tu, D. E. Raymond, J. M. Yang, H. Zhang, N. Hagen, B. Dees, E. M. Mercer, A. H. Forster, I. Kariv, P. J. Marchand and W. F. Butler, *Nat. Biotechnol.,* 2005, **23**, 83–87.
161. D. D. Carlo, D. Irimia, R. G. Tompkins and M. Toner, *Proc. Natl. Acad. Sci. U. S. A.,* 2007, **104**, 18892–18897.
162. R. D. O'Rorke, C. D. Wood, C. Walti, S. D. Evans, A. G. Davies and J. E. Cunningham, *J. Appl. Phys.,* 2012, **111**, 094911.
163. N. D. Orloff, J. R. Dennis, M. Cecchini, E. Schonbrun, E. Rocas, Y. Wang, D. Novotny, R. W. Simmonds, J. Moreland, I. Takeuchi and J. C. Booth, *Biomicrofluidics,* 2011, **5**, 044107.

164. L. Meng, F. Cai, Z. Zhang, L. Niu, Q. Jin, F. Yan, J. Wu, Z. Wang and H. Zheng, *Biomicrofluidics,* 2011, **5**, 044104.
165. X. Ding, S.-C. S. Lin, M. I. Lapsley, S. Li, X. Guo, C. Y. Chan, I.-K. Chiang, L. Wang, J. P. McCoy and T. J. Huang, *Lab Chip,* 2012, **12**, 4228–4231.
166. S. Li, X. Ding, F. Guo, Y. Chen, M. I. Lapsley, S.-C. S. Lin, L. Wang, J. P. McCoy, C. E. Cameron and T. J. Huang, *Anal. Chem.*, DOI: 10.1021/ac400548d.
167. C. D. Wood, J. E. Cunningham, R. O'Rorke, C. Wälti, E. H. Linfield, A. G. Davies and S. D. Evans, *Appl. Phys. Lett.,* 2009, **94**, 054101.
168. S. B. Q. Tran, P. Marmottant and P. Thibault, *Appl. Phys. Lett.,* 2012, **101**, 114103.
169. D. G. Grier, *Nature,* 2003, **424**, 810–816.
170. R. P. Richter, R. Bérat and A. R. Brisson, *Langmuir,* 2006, **22**, 3497–3505.
171. M. Hennig, J. Neumann, A. Wixforth, J. O. Radler and M. F. Schneider, *Lab Chip,* 2009, **9**, 3050–3053.
172. M. Hennig, M. Wolff, J. Neumann, A. Wixforth, M. F. Schneider and J. O. Radler, *Langmuir,* 2011, **27**, 14721–14725.
173. J. Neumann, M. Hennig, A. Wixforth, S. Manus, J. O. Radler and M. F. Schneider, *Nano Lett.,* 2010, **10**, 2903–2908.
174. X. H. Kong, C. Deneke, H. Schmidt, D. J. Thurmer, H. X. Ji, M. Bauer and O. G. Schmidt, *Appl. Phys. Lett.,* 2010, **96**, 134105.
175. Y. Chen, X. Ding, S.-C. S. Lin, S. Yang, P.-H. Huang, N. Nama, Y. Zhao, A. A. Nawaz, F. Guo, W. Wang, Y. Gu, T. E. Mallouk and T. J. Huang, *ACS Nano,* 2013, **7**, 3306–3314.
176. H. Li, J. Friend and L. Yeo, *Phys. Rev. Lett.,* 2008, **101**, 084502.
177. R. P. Hodgson, M. Tan, L. Y. Yeo and J. Friend, *Appl. Phys. Lett.,* 2009, **94**, 024102.
178. S. M. Langelier, L. Y. Yeo and J. Friend, *Lab Chip,* 2012, **12**, 2970–2976.